INTERNATIONAL JOURNAL FOR NUMERICAL AND ANALYTICAL METHODS IN GEOMECHANICS
Int. J. Numer. Anal. Meth. Geomech. (2016)
Published online in Wiley Online Library (wileyonlinelibrary.com). DOI: 10.1002/nag.2505

Wave propagation and strain localization in a fully saturated softening porous medium under the non-isothermal conditions

SeonHong Na and WaiChing Sun*,†

Department of Civil Engineering and Engineering Mechanics, Columbia University in the City of New York, 614 SW Mudd, Mail Code: 4709, New York, NY 10027, USA

SUMMARY

The thermo-hydro-mechanical (THM) coupling effects on the dynamic wave propagation and strain localization in a fully saturated softening porous medium are analyzed. The characteristic polynomial corresponding to the governing equations of the THM system is derived, and the stability analysis is conducted to determine the necessary conditions for stability in both non-isothermal and adiabatic cases. The result from the dispersion analysis based on the Abel–Ruffini theorem reveals that the roots of the characteristic polynomial for the THM problem cannot be expressed algebraically. Meanwhile, the dispersion analysis on the adiabatic case leads to a new analytical expression of the internal length scale. Our limit analysis on the phase velocity for the non-isothermal case indicates that the internal length scale for the non-isothermal THM system may vanish at the short wavelength limit. This result leads to the conclusion that the rate-dependence introduced by multiphysical coupling may not regularize the THM governing equations when softening occurs. Numerical experiments are used to verify the results from the stability and dispersion analyses.

Received 26 March 2015; Revised 7 December 2015; Accepted 4 January 2016

KEY WORDS: thermo-hydro-mechanics; dynamic wave propagation; stability, dispersion; internal length scale; bifurcation

1. INTRODUCTION

Localization of deformation in solids occurs in many natural processes and engineering applications. Examples of localization of deformation include the formation of Lüder and Portevin-Le Chatelier bands [1, 2] in metals and alloys, crack bands in concrete [3], and shear, compaction, and dilation bands in sand, clay, ice, and rocks [4–9]. For single-phase porous media under the static condition, the onset of strain localization is related to the loss of ellipticity, while the dynamics counterpart is due to the wave speed becoming imaginary [10–13]. These cases have been studied via stability and perturbation analyses in Hill [11, 14], which prove that perturbation grows instead of decays in unstable materials because of the ill-posedness of the governing equation. This ill-posedness of the governing equation, which can be triggered by strain softening and/or lack of normality [5], can lead to tremendous difficulty to replicate strain localization in computer simulations. One undesirable consequence is that the numerically simulated localization zones exhibit pathological dependence on the mesh size [12, 15–20]. As a result of this inherent mesh dependency, the size of mesh may affect the simulated post-bifurcation local and global responses, which do not converge upon mesh refinement [21, 22].

To circumvent this mesh dependency, a material length scale must be introduced in the governing equation. Belytschko *et al.* [23] summarized a number of ways to introduce length scale and coined them localization limiters. These methods include introducing non-local or gradient based

*Correspondence to: WaiChing Sun, Department of Civil Engineering and Engineering Mechanics, Columbia University.
†E-mail: wsun@columbia.edu

internal variables (e.g., [1, 24]), or higher-order continuum (e.g., [25–27]), and incorporating rate dependence in constitutive model (e.g., [12, 28]) to regularize the simulated responses after the onset of strain localization. This rate-dependent localization limiter is relevant to many deformation-diffusion coupling processes in multiphase materials, as the transient diffusion process is likely to introduce rate dependence to the mechanical responses due to the coupling effect. The previous works, such as Schrefler *et al*. [29, 30], Zhang and Schrefler [27], and Zhang *et al*. [31], analyze the rate-dependent effect in fluid-infiltrating porous solid via stability and dispersion analyses and derive the inherent length scale as a function of permeability and viscosity of the fluid among other material parameters. Benallal and Comi [32], Zhang and Schrefler [27], and Abellan and de Borst [33] argue that while disperse effects are indeed observed in two-phase porous media, the physical length scale introduced via hydro-mechanical coupling effect vanishes at the short wavelength limit.

Nevertheless, the aforementioned stability and dispersion analyses are based on the assumptions that the porous media is under the isothermal condition and the thermal effect is negligible and decoupled from the hydro-mechanical processes. These assumptions are reasonable for numerous engineering applications in which thermal effect plays little role on the safety or efficiency of the operations. However, THM (thermo-hydro-mechanical) coupling effect is critical for various applications, such as geothermal energy piles [34], geological disposal of carbon dioxide and nuclear wastes [35], freezing-thawing of pavement systems [36], and landslide triggered by thermal induced creeping [37].

To the best knowledge of the authors, there is no study concerning the THM coupling effect on the inherent length scale of porous media under non-isothermal condition. The purpose of this article is to fill this important knowledge gap. In particular, we apply the Routh–Hurwitz stability theorem to the THM governing equations and determine whether small perturbation can grow into localized instability and whether dispersive wave can propagate at finite wave speed in a thermal-sensitive softening porous media under the general non-isothermal condition and at the adiabatic limit. Our analysis indicates that the characteristic polynomial for the porous media under the general non-isothermal condition is of the fourth-order in the stability analysis, and of the sixth-order in the dispersion analysis. According to the Abel–Ruffini theorem (Abel's impossibility theorem), a polynomial higher than the fifth-order has no general algebraic solution. As a result, we prove that it is impossible to express the internal length scale algebraically for the general non-isothermal case. On the other hand, under the adiabatic condition, we prove that the characteristic polynomial is reduced to the third-order for the dispersion analysis. Therefore, we derive the algebraic expression of length scale for this limit case and compare both new results with the previous works on isothermal porous media [29, 33, 38].

The rest of the paper is organized as follows. We first perform the stability analysis for both general non-isothermal and adiabatic cases, and determine the onset of instability in Section 2.2. We then investigate the dispersive wave propagation in Section 2.3. In particular, we derive the phase velocity for the non-isothermal case at the long wavelength limit, and the vanishing of the physical internal length scale is observed at the short wavelength limit. For many THM coupling processes at very small time scale, the thermal conductivity of the porous media is negligible. For those adiabatic cases, we derive the simplified expression of the internal length scales and analyze the wave propagation speed during strain softening. In Section 3, we conduct numerical experiments using an 1D dynamic THM finite element code to compare and validate the analytical derivation in Sections 2.2 and 2.3. Furthermore, the influences of hydraulic properties (permeability) and thermal parameters (thermal conductivity and specific heat) on internal length scale and wave propagation behavior are evaluated for both non-isothermal and adiabatic cases, respectively. Finally, concluding remarks are given in Section 4.

As for notations and symbols, bold-faced letters denote tensors; the symbol '$\cdot$' denotes a single contraction of adjacent indices of two tensors (e.g., $a \cdot b = a_i b_i$ or $c \cdot d = c_{ij} d_{jk}$); the symbol ':' denotes a double contraction of adjacent indices of tensor of rank two or higher (e.g., $\boldsymbol{C} : \varepsilon^e = C_{ijkl}\epsilon^e_{kl}$); the symbol '$\otimes$' denotes a juxtaposition of two vectors (e.g., $\vec{a} \otimes \vec{b} = a_i b_j$) or two symmetric second order tensors (e.g., $(\vec{\alpha} \otimes \vec{\beta}) = \alpha_{ij}\beta_{kl}$). As for sign conventions, we consider the direction of the tensile stress and dilative pressure as positive.

DOI: 10.1002/nag

2. STABILITY AND DISPERSION ANALYSES

In this section, the governing equations for the wave propagation of a one-dimensional softening bar composed of fully saturated porous media under the general non-isothermal and adiabatic conditions are introduced. We perform stability and dispersion analyses on both cases and obtain the corresponding characteristic polynomials. Then, we derive the explicit expression of phase velocity and determine the vanishing length scale under long and short wavelength limits for the non-isothermal condition. In the adiabatic condition, analytical derivations of the cutoff wavenumber and internal length scale are investigated for dynamic wave propagation in a two-phase porous medium. These new results are compared with the stability and dispersion analyses for isothermal porous media.

2.1. Model assumptions and governing equations

The THM response of fluid infiltrating porous solids is governed by the balance principles, that is, the balance of linear momentum, mass, and energy. Biot [39] formulated a general thermodynamics theory for non-isothermal porous media. McTigue [40] derived a field theory for the linear thermo-elastic response of fully saturated porous media. This model is extended in Coussy [41] to incorporate the structural heating effect. Belotserkovets and Prèvost [42] derived analytical solutions of an elastic fluid-saturated porous sphere subjected to boundary heating, prescribed pore pressure, and flux. Selvadurai and Suvorov [43] analyzed the same THM problem of a spherical domain. By neglecting the heat generated and dissipated due to deformation of the solid skeleton and the flow convection of the porous spheres, the analytical solution of THM responses of the sphere composed of a fluid-saturated elasto-plastic material was derived and compared with finite element solution.

In this study, we adopt the governing equations of Coussy [41] and Belotserkovets and Prèvost [42]. We assume that the strain is infinitesimal and that there is no mass exchange between the solid and fluid constituents. The gravitational body force and heat convection of among the constituents are neglected. Furthermore, we ignored the difference between the acceleration of the fluid and solid skeleton in Eq. (1) and Eq. (2) to simplify the analysis as previously carried out in Zhang *et al*. [29], Zienkiewicz *et al*. [44]. As a result, the governing equations of the linear momentum, the fluid mass balance, and the energy balance read,

$$\nabla \cdot \left(\sigma' - bp - \beta T\right) - \rho \ddot{u} = 0, \tag{1}$$

$$b\nabla \cdot \dot{u} - k\nabla^2 p + \frac{1}{M}\dot{p} - 3\alpha_m \dot{T} = 0, \tag{2}$$

$$\rho c \dot{T} - \kappa \nabla^2 T + T_0 \beta \nabla \cdot \dot{u} - 3\alpha_m T_0 \dot{p} = 0, \tag{3}$$

where σ' is effective stress (nominal effective stress in Liu *et al*. [45]), p is pore pressure, T is temperature, u is displacement of solid skeleton, and b is the Biot's coefficient. The mobility, k, is defined as $k = k_s/\mu_f = k_{perm}/\rho_f g$, in which k_s is the intrinsic permeability, μ_f is the fluid viscosity, k_{perm} is the permeability or hydraulic conductivity, and g is the gravity acceleration. Furthermore, T_0 is the reference temperature as defined in [42]. β is calculated as $\beta = 3\alpha_s K$, in which α_s is the linear thermal expansion coefficient of solid, and K is the bulk modulus. Also, the volume averaged thermal expansion coefficient α_m is expressed as $\alpha_m = (b-n)\alpha_s + n\alpha_f$, a function of porosity n and the linear thermal expansion coefficient of fluid α_f. Here, $\rho = (1-n)\rho_s + n\rho_f$, in which ρ_s and ρ_f are solid and fluid mass densities, κ is the thermal conductivity, and c_s, c_f are the specific heat per unit mass of solid and fluid. The Biot's modulus is denoted as M, which is a function of the Biot's coefficient b, porosity n, the bulk modulus of the solid grain K_s, and that of the fluid constituent K_f, that is,

$$\frac{1}{M} = \frac{b-n}{K_s} + \frac{n}{K_f}. \tag{4}$$

In this study, the volume-averaged specific heat of the constituents, $\rho c = (1-n)\rho_s c_s + n\rho_f c_f$, is considered to be specific heat of two-phase fluid–solid mixture. In addition, we assume that the

DOI: 10.1002/nag

temperature is at equilibrium locally and hence there is no temperature difference between the two constituents at the same material point. To simplify the stability and dispersion analyses, we limit our attention to a one-dimensional dynamic THM boundary value problem.

2.2. *Stability analysis*

In this section, we analyze stability of a one-dimensional wave propagation in a thermal-sensitive fluid-saturated porous media. Our goal here is to determine the necessary and sufficient conditions to maintain stability of the THM system in the generalized non-isothermal case and at the adiabatic limit. Our results are compared with the previous analyses on isothermal porous media. In particular, we apply the Routh–Hurwitz stability theorem to the characteristic equations of the general non-isothermal and adiabatic THM systems. The Routh–Hurwitz criterion enables us to determine whether it is possible that the solution of characteristic equation can have a real and positive part, which in return implies that homogeneous state is unstable and a small perturbation may grow [1].

2.2.1. Non-isothermal case. To investigate the stability of an equilibrium state, we apply a harmonic perturbation with respect to an incremental axial displacement, pore pressure, and temperature. For an infinite one-dimensional thermo-sensitive porous medium initially in a homogeneous state, the solution of displacement, pore pressure, and temperature in space-time (x, t) may take the following form,

$$\begin{bmatrix} du \\ dp \\ dT \end{bmatrix} = \begin{bmatrix} A_u \\ A_p \\ A_T \end{bmatrix} e^{i(k_w x - \omega t)} = A e^{i k_w x + \lambda t},\ \lambda = -i\omega, \tag{5}$$

where k_w is the wavenumber, ω the angular frequency, and λ eigenvalue. A_u, A_p, and A_T are the amplitudes of the displacement, pore pressure, and temperature perturbations, respectively. Following the approach in Zhang *et al*. [29] and Abellan and de Borst [33], we use an incremental linear constitutive model to relate the infinitesimal change of the nominal effective stress and that of the total strain for the one-dimensional THM problem, that is,

$$\dot{\sigma}' = E_t \frac{\partial \dot{u}}{\partial x} = E_t \dot{\varepsilon}, \tag{6}$$

where E_t is the tangential stiffness modulus of the solid (cf. Abellan and de Borst [33]). The relations among the one-dimensional total stress σ, Biot's effective stress σ'', and the nominal effective stress σ' are [45],

$$\dot{\sigma} = \dot{\sigma}'' - b\dot{p} = \dot{\sigma}' - \beta \dot{T} - b\dot{p}. \tag{7}$$

The spatial derivative of the incremental nominal effective stress Eq. (6) gives

$$\frac{\partial \dot{\sigma}'}{\partial x} = -E_t A_u k_w^2 \exp(i k_w x + \lambda t). \tag{8}$$

The substitution of Eq. (5) into Eqs. (1) to (3) therefore gives

$$-E_t k_w^2 A_u - i(b k_w) A_p - i(\beta k_w) A_T - \rho \lambda^2 A_u = 0, \tag{9}$$

$$i(b k_w \lambda) A_u + k k_w^2 A_p + M^{-1} \lambda A_p - 3\alpha_m \lambda A_T = 0, \tag{10}$$

$$\rho c \lambda A_T + \kappa k_w^2 A_T + i(T_0 \beta k_w \lambda) A_u - 3\alpha_m T_0 \lambda A_p = 0. \tag{11}$$

A non-trivial solution to this set of homogeneous equations exists if and only if the following relation holds

$$\begin{vmatrix} -E_t k_w^2 - \rho\lambda^2 & -i(b k_w) & -i(\beta k_w) \\ i(b k_w \lambda) & k k_w^2 + M^{-1}\lambda & -3\alpha_m \lambda \\ i(T_0 \beta k_w \lambda) & -3\alpha_m T_0 \lambda & \rho c \lambda + \kappa k_w^2 \end{vmatrix} = 0, \tag{12}$$

DOI: 10.1002/nag

which can be rewritten as shown in the succeeding equation,

$$\begin{aligned}\left(-E_t k_w^2-\rho\lambda^2\right)\left[\left(kk_w^2+M^{-1}\lambda\right)\left(\rho c\lambda+\kappa k_w^2\right)-(-3\alpha_m\lambda)\left(-3\alpha_m T_0\lambda\right)\right]\\ +i(bk_w)\left[i(bk_w\lambda)(\rho c\lambda+\kappa k_w^2)-(-3\alpha_m\lambda)\left(i\left(T_0\beta k_w\lambda\right)\right)\right]\\ -i(\beta k_w)\left[i\left(bk_w\lambda\right)\left(-3\alpha_m T_0\lambda\right)-\left(kk_w^2+M^{-1}\lambda\right)\left(i\left(T_0\beta k_w\lambda\right)\right)\right]=0.\end{aligned} \tag{13}$$

Expanding Eq. (13) yields

$$\begin{aligned}-\frac{1}{M}\rho^2 c\lambda^4+9\alpha_m^2\rho T_0\lambda^4-\frac{1}{M}\rho\kappa k_w^2\lambda^3-\rho^2 ck_w^2\lambda^3-\frac{1}{M}\rho cE_t k_w^2\lambda^2-\rho cb^2k_w^2\lambda^2\\ -\rho\kappa kk_w^4\lambda^2-\frac{1}{M}\beta^2T_0k_w^2\lambda^2-6\alpha_m\beta bT_0k_w^2\lambda^2+9E_t\alpha_m^2T_0k_w^2\lambda^2\\ -\frac{1}{M}E_t\kappa k_w^4\lambda-b^2\kappa k_w^4\lambda-\rho cE_tkk_w^4\lambda-\beta^2kT_0k_w^4\lambda-E_tk\kappa k_w^6=0,\end{aligned} \tag{14}$$

in which the terms in Eq. (14) are rearranged in descending order for eigenvalue, λ. Simplifying the expression of Eq. (14) yields ($M\neq 0$),

$$\begin{aligned}\rho(\rho c-9\alpha_m^2T_0M)\lambda^4+\rho(\kappa+\rho ckM)k_w^2\lambda^3+(\rho cE_t+\rho cb^2M+\rho\kappa kMk_w^2\\ +\beta^2T_0+6\alpha_m\beta bT_0M-9E_t\alpha_m^2T_0M)k_w^2\lambda^2\\ +(E_t\kappa+b^2\kappa M+\rho cE_tkM+\beta^2kT_0M)k_w^4\lambda+E_tk\kappa Mk_w^6=0.\end{aligned} \tag{15}$$

After rearranging Eq. (15), the characteristic equation is a forth-order polynomial that reads,

$$a_4\lambda^4+a_3\lambda^3+a_2\lambda^2+a_1\lambda+a_0=0, \tag{16}$$

with the following real coefficients,

$$a_4=\rho(\rho c-9\alpha_m^2T_0M), \tag{17}$$

$$a_3=\rho(\kappa+\rho ckM)k_w^2, \tag{18}$$

$$a_2=\left(\rho cE_t+\rho cb^2M+\rho\kappa kMk_w^2+\beta^2T_0+6\alpha_m\beta bT_0M-9E_t\alpha_m^2T_0M\right)k_w^2, \tag{19}$$

$$a_1=\left(E_t\kappa+b^2\kappa M+\rho cE_tkM+\beta^2kT_0M\right)k_w^4, \tag{20}$$

$$a_0=E_tk\kappa Mk_w^6. \tag{21}$$

According to the Routh–Hurwitz stability criterion, the stability of the governing equations is maintained if and only if all the solutions of characteristic polynomial have negative real part [46, 47]. For the fourth-order polynomial shown in Eq. (16), the necessary condition to satisfy the Routh–Hurwitz stability criterion is to have the coefficients listed in Eqs. (17) to (21) hold the following properties,

$$a_n>0,\ a_3a_2>a_4a_1,\ \text{and}\ a_3a_2a_1>a_4a_1^2+a_3^2a_0\ \text{, where}\ n=0,1,2,3,4. \tag{22}$$

We first examine Eq. $(22)_1$, which requires all coefficients $a_i, i=0,1,2,3,4$, to be strictly positive. Notice that these coefficients are all the functions of the material parameters that characterize the mechanical, hydraulic, and thermal responses of porous media. As a result, one may deduce the necessary condition to satisfy Eq. $(22)_1$ by examining the physical meaning and the possible ranges of the material parameters. Here, we categorize the material parameters into three groups – strictly positive, non-negative, and real number (which can be negative, zero, or positive). Among these three groups, we first assume that the total density ρ, specific heat c, Biot's modulus M, and Biot's coefficient b are all strictly positive and hence greater than zero. Meanwhile, the mobility k, thermal conductivity κ, thermal expansion coefficient α_m, and the reference temperature T_0 are assumed to

DOI: 10.1002/nag

Table I. Assumptions on range of the material properties of thermo-sensitive porous media.

Parameter	Description	Range
ρ	Total Density	$\mathbb{R}^+$
c	Specific Heat	$\mathbb{R}^+$
M	Biot's Modulus	$\mathbb{R}^+$
b	Biot's Coefficient	(0,1]
k	Mobility	$[0, \infty)$
κ	Thermal Conductivity	$[0, \infty)$
α	Thermal Expansion Coefficient	$[0, \infty)$
T_0	Reference Temperature	$[0, \infty)$
E_t	Tangential Modulus	$\mathbb{R}$

be non-negative (if the temperature unit is Kelvin). Finally, the tangential stiffness E_t can be both positive, negative, or zero, as summarized in Table I.

With the aforementioned assumptions in mind, we notice that a_0, a_1, and a_3 may all become non-positive when both thermal conductivity and permeability of the material become zero. This result indicates that the wave propagating in non-isothermal porous medium may lose stability at the undrained limit even though there is no softening. At the adiabatic limit, we found that one of the roots of the characteristic polynomial is zero and at least one of the root may have a positive real part if at least one of the four conditions listed at the end of Section 2.2.2 is met. On the other hand, a_4 is greater than zero if both solid and fluid constituents do not exhibit thermal expansion such that $\alpha_m = 0$. However, to maintain stability, the specific heat must be large enough such that $c > 9\alpha_m^2 T_0 M/\rho$. In other words, from a theoretical standpoint, it is possible for the THM governing equations to lose stability if the fluid and solid constituents are both nearly incompressible but the porous medium is vulnerable to significant thermal expansion (e.g., marine clay). This indicates that material softening is not the only indicator that detects the loss of stability in the THM problem. Furthermore, a necessary and sufficient condition for $a_0 > 0$, $a_1 > 0$, and $a_2 > 0$ is to have $E_t > 0$, that is, no softening occurring. A few algebraic operations reveal that,

$$a_2 > 0 \text{ implies that } E_t > \frac{-\rho c b^2 M - \rho\kappa k M k_w^2 - \beta^2 T_0 - 6\alpha_m \beta b T_0 M}{\rho c - 9\alpha_m^2 T_0 M}, \tag{23}$$

$$a_1 > 0 \text{ implies that } E_t > \frac{-b^2\kappa M - \beta^2 k T_0 M}{\kappa + \rho c k M}. \tag{24}$$

Because the stability condition also requires $a_4 > 0$ and hence $\rho c - 9\alpha_m^2 T_0 M > 0$, both (23) and (24) would not be violated unless softening occurs (i.e., $E_t < 0$). Meanwhile, the explicit expression of $a_3 a_2 > a_4 a_1$ reads,

$$\begin{aligned} k\kappa^2 M\rho^2 k_w^6 + b^2 c^2 k M^2 \rho^3 k_w^4 + c k^2 \kappa M^2 \rho^3 k_w^6 + \beta^2 \kappa \rho T_0 k_w^4 + 6\alpha_m b \beta \kappa M \rho T_0 k_w^4 \\ + 9\alpha_m^2 b^2 \kappa M^2 \rho T_0 k_w^4 + 6\alpha_m b \beta c k M^2 \rho^2 T_0 k_w^4 + 9\alpha_m^2 \beta^2 k M^2 \rho T_0^2 k_w^4 > 0, \end{aligned} \tag{25}$$

which can be expressed as in the succeeding equation,

$$\rho k_w^4 \left[\rho^2 c k^2 \kappa M^2 k_w^2 + \kappa T_0 (\beta + 3b\alpha_m M)^2 + kM\left(\rho\kappa^2 k_w^2 + M(b\rho c + 3\beta\alpha_m T_0)^2\right)\right] > 0. \tag{26}$$

Condition (26) always holds if the wavenumber is real, either the permeability or the thermal conductivity is non-zero and the rest of the material parameters are strictly positive. Finally, $a_3 a_2 a_1 > a_4 a_1^2 + a_3^2 a_0$ can be expanded as,

DOI: 10.1002/nag

$$
\begin{aligned}
b^2k\kappa^3M^2\rho^2k_w^{10} &+ b^2c^2E_tk\kappa M^2\rho^3k_w^8 + b^4c^2k\kappa M^3\rho^3k_w^8 + b^2ck^2\kappa^2M^3\rho^3k_w^{10}\\
&+ b^2c^3E_tk^2M^3\rho^4k_w^8 + \beta^2E_t\kappa^2T_0\rho k_w^8 + b^2\beta^2\kappa^2MT_0\rho k_w^8\\
&+ 6\alpha_mb\beta E_t\kappa^2MT_0\rho k_w^8 + 6\alpha_mb^3\beta\kappa^2M^2T_0\rho k_w^8 + 9\alpha_m^2b^2E_t\kappa^2M^2T_0\rho k_w^8\\
&+ 9\alpha_m^2b^4\kappa^2M^3T_0\rho k_w^8 + \beta^2cE_tk\kappa MT_0\rho^2k_w^8 + 12\alpha_mb\beta cE_tkM^2T_0\kappa\rho^2k_w^8\\
&+ \beta^2k^2\kappa^2M^2T_0\rho^2k_w^{10} + 6\alpha_mb^3\beta ck\kappa M^3T_0\rho^2k_w^8 + 9\alpha_m^2b^2cE_tk\kappa M^3T_0\rho^2k_w^8\\
&+ b^2\beta^2c^2k^2M^3T_0\rho^3k_w^8 + 6\alpha_mb\beta c^2E_tk^2M^3T_0\rho^3k_w^8 + \beta^2ck^3\kappa M^3T_0\rho^3k_w^{10}\\
&+ \beta^4k\kappa MT_0^2\rho k_w^8 + 6\alpha_mb\beta^3k\kappa M^2T_0^2\rho k_w^8 + 9\alpha_m^2\beta^2E_tk\kappa M^2T_0^2\rho k_w^8\\
&+ 18\alpha_m^2b^2\beta^2k\kappa M^3T_0^2\rho k_w^8 + 6\alpha_mb\beta^3ck^2M^3T_0^2\rho^2k_w^8\\
&+ 9\alpha_m^2\beta^2cE_tk^2M^3T_0^2\rho^2k_w^8 + 9\alpha_m^2\beta^4k^2M^3T_0^3\rho k_w^8 > 0,
\end{aligned}
\tag{27}
$$

which can be further simplified as

$$
\begin{aligned}
&E_t\rho k_w^8(\kappa+\rho ckM)\left[6\alpha_mb\beta MT_0(\kappa+\rho ckM) + b^2M^2\left(\rho^2c^2k + 9\alpha_m^2\kappa T_0\right)\right.\\
&\left.+\beta^2T_0\left(\kappa + 9\alpha_m^2kM^2T_0\right)\right] + \rho k_w^8M\left(b^2\kappa+\beta^2kT_0\right)\left[\rho^2ck^2\kappa M^2k_w^2 + \kappa T_0(\beta+3\alpha_mbM)^2\right.\\
&\left.+kM\left(\kappa^2\rho k_w^2 + M(\rho cb+3\alpha_m\beta T_0)^2\right)\right] > 0.
\end{aligned}
\tag{28}
$$

In other words, $a_3a_2a_1 > a_4a_1^2 + a_3^2a_0$ implies that

$$
E_t > \frac{-M(b^2\kappa+\beta^2kT_0)\left[\rho^2ck^2\kappa M^2k_w^2 + \kappa T_0(\beta+3\alpha_mbM)^2 + kM\left(\kappa^2\rho k_w^2 + M(\rho cb+3\alpha_m\beta T_0)^2\right)\right]}{(\kappa+\rho ckM)\left[6\alpha_mb\beta MT_0(\kappa+\rho ckM) + b^2M^2\left(\rho^2c^2k+9\alpha_m^2\kappa T_0\right) + \beta^2T_0\left(\kappa+9\alpha_m^2kM^2T_0\right)\right]},
\tag{29}
$$

which would not be violated unless softening occurs (i.e., $E_t < 0$) as the aforementioned Eqs. (23) and (24).

As a result, the THM governing equations may fail the Routh–Hurwitz criterion if at least one of the following situations happens:

1. Softening occurs such that $E_t < 0$.
2. Both permeability and thermal conductivity of the porous media become zero.
3. Specific heat $c \le 9\alpha_m^2T_0M/\rho$.

2.2.2. Adiabatic case. The stability analysis conducted in the previous section can be significantly simplified by assuming that the entire one-dimensional bar is in the adiabatic or isothermal condition. While the latter case has been extensively studied in the past (cf. Abellan and de Borst [29], Zhang and Schrefler [27, 38], Zhang *et al*. [33]), the stability analysis of adiabatic porous media has not yet been established. For many engineering applications in which high-rate and shock responses are of interest, it is reasonable to assume that the thermal conductivity is negligible. In those cases, we may derive the characteristic equation for the adiabatic condition by assuming the thermal conductivity to be zero, $\kappa \approx 0$. As a result, the characteristic equation of the adiabatic THM system reads,

$$
\begin{vmatrix}
-E_tk_w^2 - \rho\lambda^2 & -i(bk_w) & -i(\beta k_w)\\
i(bk_w\lambda) & kk_w^2 + M^{-1}\lambda & -3\alpha_m\lambda\\
i(T_0\beta k_w\lambda) & -3\alpha_mT_0\lambda & \rho c\lambda
\end{vmatrix} = 0,
\tag{30}
$$

which can be rewritten as shown in the next equation,

$$
\begin{aligned}
&\left(-E_tk_w^2-\rho\lambda^2\right)\left[\left(kk_w^2+M^{-1}\lambda\right)\rho c\lambda - (-3\alpha_m\lambda)(-3\alpha_mT_0\lambda)\right]\\
&\qquad +i(bk_w)\left[i(bk_w\lambda)\rho c\lambda - (-3\alpha_m\lambda)\left(i\left(T_0\beta k_w\lambda\right)\right)\right]\\
&-i(\beta k_w)\left[i(bk_w\lambda)(-3\alpha_mT_0\lambda) - \left(kk_w^2+M^{-1}\lambda\right)\left(i\left(T_0\beta k_w\lambda\right)\right)\right] = 0.
\end{aligned}
\tag{31}
$$

DOI: 10.1002/nag

Expanding Eq. (31) yields

$$\begin{aligned}&-\frac{1}{M}\rho^2 c\lambda^4+9\rho\alpha_m^2 T_0\lambda^4-\rho^2 ckk_w^2\lambda^3-\frac{1}{M}\rho cE_t k_w^2\lambda^2-\rho cb^2k_w^2\lambda^2\\&-\frac{1}{M}\beta^2T_0k_w^2\lambda^2-6\alpha_m\beta bT_0k_w^2\lambda^2+9E_t\alpha_m^2T_0k_w^2\lambda^2\\&-\rho cE_tkk_w^4\lambda-\beta^2kT_0k_w^4\lambda=0,\end{aligned}\tag{32}$$

which can be rewritten as

$$\begin{aligned}-\frac{1}{M}\lambda\left[\rho\left(\rho c-9\alpha_m^2T_0M\right)\lambda^3+\rho^2ckMk_w^2\lambda^2+\left(\rho cE_t+\rho cb^2M+\beta^2T_0+6\alpha_m\beta bT_0M\right.\right.\\\left.\left.-9E_t\alpha_m^2T_0M\right)k_w^2\lambda+\left(\rho cE_t+\beta^2T_0\right)kMk_w^4\right]=0.\end{aligned}\tag{33}$$

This equation can be expressed into a more compacted form that reads ($M\neq 0$),

$$b_3\lambda^4+b_2\lambda^3+b_1\lambda^2+b_0\lambda=0\ \text{ or }\ (b_3\lambda^3+b_2\lambda^2+b_1\lambda+b_0)\lambda=0,\tag{34}$$

where the expressions of the coefficients are

$$b_3=\rho\left(\rho c-9\alpha_m^2T_0M\right),\tag{35}$$

$$b_2=\rho^2ckMk_w^2,\tag{36}$$

$$b_1=\left(\rho cE_t+\rho cb^2M+\beta^2T_0+6\alpha_m\beta bT_0M-9\alpha_m^2E_tT_0M\right)k_w^2,\tag{37}$$

$$b_0=\left(\rho cE_t+\beta^2T_0\right)kMk_w^4.\tag{38}$$

At the adiabatic limit, the vanishing of the Laplacian term in the balance of energy equation leads to a fourth-order characteristic polynomial Eq. (34) of which one of the roots is obviously zero ($\lambda=0$). This root represents a neutrally stable condition in which perturbation neither grows (which requires a positive real part) or decay (which requires a negative real part) [1]. To determine whether perturbation may grow, we examine the rest of the roots corresponding to Eq. (34) and analyze the ranges of material parameters that lead to at least one root having a positive real part (and hence causes a perturbation to grow). Note that the coefficients $b_i, i=0,1,2,3$ in Eq. (34) are either functions of an exponentiation of the wavenumber of a particular order, that is, k_w^2, k_w^4, or independent of k_w. Furthermore, these coefficients do not depend on the exponentiation of the wavenumber with multiple orders as a_2 in Eq. (19). This feature allows one to derive the cutoff wavenumber, which provides the range of wavenumbers where wave propagation is possible in the adiabatic porous media.

Now, apply the Routh–Hurwitz stability criterion to the polynomial corresponding to the non-zero roots, that is, $b_3\lambda^3+b_2\lambda^2+b_1\lambda+b_0=0$. The necessary condition to satisfy the Routh–Hurwitz stability criterion reads

$$b_n>0 \text{ and } b_2b_1>b_3b_0\ \text{, where }\ n=0,1,2,3,\tag{39}$$

where $b_2b_1-b_3b_0>0$ can be written as

$$\rho kM^2\left(\rho cb+3\alpha_m\beta T_0\right)^2k_w^4>0.\tag{40}$$

This condition holds when the mobility k is positive. In analogy to the general non-isothermal case, we can identify the necessary condition that leads to instability. The loss of stability may appear if one of the following criteria is met:

1. Mobility $k=0$, in which case b_0 and b_2 are both equal to 0.
2. Tangential modulus $E_t\leq-(\beta^2T_0/\rho c)$ leads to $b_0\leq 0$.

DOI: 10.1002/nag

3. Tangential modulus $E_t \leq -(\rho c b^2 M + \beta^2 T_0 + 6\alpha_m \beta b T_0 M)/(\rho c - 9\alpha_m^2 T_0 M)$ leads to $b_1 \leq 0$.
4. Specific heat $c \leq 9\alpha_m^2 T_0 M/\rho$ so that $b_3 \leq 0$.

Remark 1
Notice that in many THM formulations, such as Selvadurai and Suvorov [43] and Selvadurai and Suvorov [48], the work carried out or energy dissipation of the fluid and solid constituents are assumed to be negligible in the balance of energy equation. In this case, the energy balance equation, Eq. (3), may be simplified as

$$\dot{T} - \frac{\kappa}{\rho c}\frac{\partial^2 T}{\partial x^2} = 0. \tag{41}$$

Hence, the mechanical and hydraulic responses are only one-way coupled with the heat transfer process. While the temperature changes may still cause deformation and/or flow, Eq. (41) indicates that neither deformation of the solid skeleton or the pore-fluid flow may impose any influence on the temperature due to the simplified assumptions. In this special case, the characteristic equation reads,

$$\begin{vmatrix} -E_t k_w^2 - \rho\lambda^2 & -i(bk_w) & -i(\beta k_w) \\ i(bk_w\lambda) & k k_w^2 + M^{-1}\lambda & -3\alpha_m\lambda \\ 0 & 0 & \rho c\lambda + \kappa k_w^2 \end{vmatrix} = 0. \tag{42}$$

In the one-way coupling THM formulations, the characteristic equation will have two roots identical with those in the fully saturated isothermal condition [29, 33, 38], while the additional root is $\lambda = -\kappa k_w^2/(\rho c)$, which is either equal to zero (when $\kappa = 0$) or negative (when κ is positive). In other words, if the thermal conductivity is non-zero, then the governing equations of the one-way coupling THM system and the isothermal THM system share the same necessary and sufficient conditions for stability.

2.3. Dispersion analysis

Even if stability is lost, numerical simulations may still continue and give meaningful results as pointed out by Abellan and de Borst [33]. However, when the THM problem becomes ill-posed, the physical length scale inferred from the physical properties vanishes, and a numerical length scale, which is often the mesh size, may influence the numerical solutions and cause mesh dependency. The dispersion analysis provides a tool to predict the vanishing of finite non-zero physical wavelength by checking whether the associated cutoff wavenumber or damping factor can be identified. Recall that a wave is considered dispersive if the phase velocity (or wave velocity, v_p) depends on the wavenumber [27, 29, 32, 33, 38, 49–52]. In this case, the waves of different wavelengths travel at different phase velocities, and hence, the shape of a dispersive wave may change as it propagates [53]. To capture localization of deformation properly, governing equation must be able to change the shape of an arbitrary loading wave into a stationary wave in a localization zone [18, 33]. It is well known that wave propagation in the standard single-phase continuum upon the occurrence of strain softening is not dispersive, and hence, the mesh dependency is observed [1, 33].

In this section, our objectives are to (i) investigate whether a dispersive wave can propagate at the long and short wavelength limits in the non-isothermal case, and (ii) examine the cutoff wavenumber and internal length scale when strain softening at the adiabatic limit.

2.3.1. Non-isothermal case. We assume that the solution of the governing equations of a damped, harmonic wave propagating in a thermo-sensitive fully saturated two-phase porous media takes the following form:

$$\begin{bmatrix} du \\ dp \\ dT \end{bmatrix} = \begin{bmatrix} A_u \\ A_p \\ A_T \end{bmatrix} e^{i(k_w x - \omega t)} = A e^{\lambda_r t + i(k_w x - \omega t)}, \tag{43}$$

DOI: 10.1002/nag

where A_u, A_p, and A_T are the amplitudes of the displacement, pore pressure, and temperature accordingly. In the dispersion analysis, we split the possible complex eigenvalue into real part (λ_r) and imaginary party (ω or λ_i) as $\lambda = \lambda_r - i\omega$. According to Zhang *et al.* [29] and the dispersion analysis of adiabatic case later, the cutoff wavenumber can be derived using the discriminant of cubic polynomial of eigenvalue when the same order of wavenumber term exists in each coefficient of the characteristic equation (e.g., Eq. (34)). However, in the characteristic equation of non-isothermal condition (Eq. (16)), the coefficient a_2 has two different orders of wavenumber (k_w^2 and k_w^4), and the derivation of discriminant of quartic polynomial cannot give the explicit expression of wavenumber having the complex conjugate roots. Nevertheless, we may still determine the relation between the phase velocity and the real and imaginary parts of the eigenvalue by substituting $\lambda = \lambda_r - i\omega$ into Eq. (16). This process, based on Abellan and de Borst [33], decomposes the characteristic equation into real and imaginary parts as follows,

$$\begin{aligned} &a_4\lambda_r^4 + a_3\lambda_r^3 + a_2\lambda_r^2 + a_1\lambda_r + a_0 - a_2\omega^2 - 3a_3\lambda_r\omega^2 - 6a_4\lambda_r^2\omega^2 + a_4\omega^4 \\ &\quad + i\left(-a_1\omega - 2a_2\lambda_r\omega - 3a_3\lambda_r^2\omega - 4a_4\lambda_r^3\omega + a_3\omega^3 + 4a_4\lambda_r\omega^3\right) = 0. \end{aligned} \tag{44}$$

The imaginary part of Eq. (44) vanishes if the following condition holds,

$$\omega = 0 \text{ or } \omega^2 = \frac{4a_4\lambda_r^3 + 3a_3\lambda_r^2 + 2a_2\lambda_r + a_1}{+4a_4\lambda_r + a_3}. \tag{45}$$

For the dispersion analysis of dynamic governing equations, we can assume $\omega \neq 0$ and take the condition of Eq. $(45)_2$. By considering the coefficients $a_i, i = 0, 1, 2, 3, 4$ of Eqs. (17) to (21), we know that ω is expressed in terms of wavenumber (k_w), and the relation of phase velocity ($v_p = \omega/k_w$) and wavenumber can be derived (Appendix A). Because the phase velocity is dependent on the wavenumber, we can find out that the wave propagation is dispersive. Furthermore, by substituting Eq. $(45)_2$ into Eq. (44), the equation of real part of eigenvalue λ_r can be expressed as shown in the succeeding equation,

$$\begin{aligned} &\left[64a_4^3\lambda_r^6 + 96a_3a_4^2\lambda_r^5 + \left(48a_3^2a_4 + 32a_2a_4^2\right)\lambda_r^4 + \left(8a_3^3 + 32a_2a_3a_4\right)\lambda_r^3\right. \\ &\quad + (8a_2a_3^2 + 4a_2^2a_4 + 4a_1a_3a_4 - 16a_0a_4^2)\lambda_r^2 + \left(2a_2^2a_3 + 2a_1a_3^2 - 8a_0a_3a_4\right)\lambda_r \\ &\quad \left. + a_1a_2a_3 - a_0a_3^2 - a_1^2a_4\right] / \left(16a_4^2\lambda_r^2 + 8a_4a_3\lambda_r + a_3^2\right) = 0. \end{aligned} \tag{46}$$

Unfortunately, as proven by the Abel–Ruffini theorem (also referred as the Abel's impossibility theorem [54]), there exists no **general** algebraic solution in radicals to polynomials of degree five or higher with arbitrary coefficients. In other words, there is no general formula that allows the real part of eigenvalue λ_r to be expressed algebraically, even though it is still possible to solve Eq. (46) numerically. However, we can estimate λ_r by taking long and short wavelength limits considering the coefficients $a_i, i = 0, 1, 2, 3, 4$ and Eqs. (45) to (46).

Firstly, we found that taking the long wavelength limit, that is, $k_w \to 0$, yields the eigenvalue $\lambda_r \to 0$ in Eq. (46). As demonstrated in Abellan and de Borst [33], this result leads to the relation of phase velocity and wavenumber according to Eq. $(45)_2$. Therefore, we can explicitly derive the phase velocity for the long wavelength limit as shown below.

$$v_p = \sqrt{\frac{E_t\kappa + b^2\kappa M + \rho c E_t k M + \beta^2 k T_0 M}{\rho(\kappa + \rho c k M)}} = \sqrt{\frac{E_t}{\rho} + \frac{b^2\kappa M}{\rho(\kappa + \rho c k M)} + \frac{\beta^2 T_0 k M}{\rho(\kappa + \rho c k M)}}. \tag{47}$$

Observe that the phase velocity of Eq. (47) is reduced to the classical bar velocity, $v_p = \sqrt{E_t/\rho}$, κ and k are negligible. Figure 1 shows how the phase velocity changes depending on the thermal conductivity and permeability (or mobility k), where the material properties are selected from the previous studies (Sun [22], Zhang *et al.* [29]). When the thermal conductivity is given, for example $\kappa = 2.5 \times 10^{-3}$ kW/m/°C, the phase velocity does not change until the permeability decreases below $k_{perm} \approx 1.0 \times 10^{-6}$ m/s. Besides, when the permeability is further decreased and beyond the range, $1.0 \times 10^{-8} < k_{perm} < 1.0 \times 10^{-6}$ (m/s), additional response from the phase

DOI: 10.1002/nag

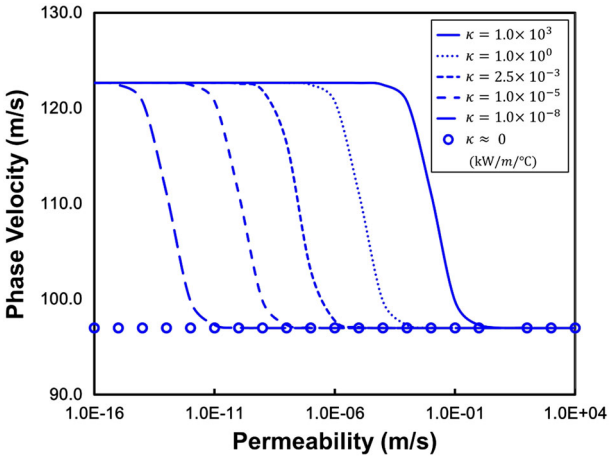

Figure 1. Phase velocity versus permeability with different thermal conductivities (With $E_t = 30$ MPa, $\rho c = 4.5$ kJ/m^3/°C, M = 200 MPa and $T_0 = 20$ °C).

velocity is not observed. In other words, the phase velocity of the THM system can be influenced by how the permeability and thermal conductivity are combined, but the effect is limited.

For the short wavelength limit, that is, $k_w \to \infty$, we can estimate that $\lambda_r \sim k_w^{10}$ from Eq. (46) and the wave velocity become proportional to the wavenumber, $v_p \sim k_w$, from Eq. (45). By adopting the relation of the internal length scale and damping coefficient from a single-phase rate-dependent medium [53], the internal length scale (l) is defined as follows:

$$l = \lim_{k_w \to \infty} \left(-\frac{v_p}{\lambda_r} \right) \sim \lim_{k_w \to \infty} k_w^{-9} = 0. \tag{48}$$

This means that the internal length scale vanishes at the short wavelength limit. The loss of physical internal length scale also suggests that any grid-based numerical model that solves the THM governing equations may exhibit mesh dependency, as any regularization effect induced by multi-physical coupling may vanish if the physical length scale vanished.

In other words, the rate-dependence introduced through multiphysical coupling may not regularize the THM governing equations when softening occurs. This conclusion echoes the previous dispersion analysis of isothermal two-phase porous media by Abellan and de Borst [33], which also indicates that the internal length scale vanishes at the short wavelength limit. The wave propagation behavior of non-isothermal condition when strain softening occurs is further evaluated by numerical experiments in Section 3.2.

For the adiabatic case, we derived the internal length scale of the adiabatic THM system within a limited range of wavenumbers by expanding the derivation for isothermal porous system in Zhang *et al*. [29]. In addition, we conducted parametric studies to analyze how the specific heat and permeability may affect the cutoff wavenumber and the corresponding internal length scale.

2.3.2. Adiabatic Case. By assuming that the thermal conductivity is approximately zero, we obtained the characteristic equation of a damped harmonic wave propagating in a porous medium at the adiabatic limit. Based on the derivations in Section 2.2.2, we conducted a dispersion analysis and derive the expression of the internal length scale when the porous medium remains at the adiabatic limit. Our starting point is the third-order characteristic polynomial, which takes the following form,

$$D(\lambda) = \lambda^3 + a\lambda^2 + b\lambda + c = 0, \tag{49}$$

where

$$a = a^0 y, \quad a^0 = \frac{\rho c k M}{\rho c - 9\alpha_m^2 T_0 M}, \tag{50}$$

DOI: 10.1002/nag

$$b = b^0 y, \;\; b^0 = \frac{\rho c E_t + \rho c b^2 M + \beta^2 T_0 + 6\alpha_m \beta b T_0 M - 9\alpha_m^2 E_t T_0 M}{\rho\left(\rho c - 9\alpha_m^2 T_0 M\right)}, \tag{51}$$

$$c = c^0 y^2, \;\; c^0 = \frac{\left(\rho c E_t + \beta^2 T_0\right) k M}{\rho\left(\rho c - 9\alpha_m^2 T_0 M\right)}, \tag{52}$$

$$y = k_w^2. \tag{53}$$

When strain softening occurs, the tangential modulus E_t becomes negative. In this case, waves propagating in the porous medium can be either dispersive or non-dispersive, depending on the wavenumber k_w.

Our objective here is to determine whether it is possible to propagate waves with finite speed when stability of the THM system has already been lost. Recall that the stability analysis in Section 2.2.2 indicates loss of stability when either one of the following conditions holds, that is, (1) $E_t < -(\beta^2 T_0/\rho c)$, (2) $c > 9\alpha_m^2 T_0 M/\rho$, (3) $k = \kappa = 0$. Here, we assume that the permeability is non-zero and focus our attention only on the cases in which condition (1) and (2) hold. Furthermore, we assume that the softening tangential modulus $E_t > -b^2 M$ always holds [14, 29]. In other words, our objective is to determine whether the roots of the characteristic polynomial contain positive real part for the special case where the following condition holds,

$$-b^2 M < E_t < -\beta^2 T_0/\rho c, \;\; c > 9\alpha_m^2 T_0 M/\rho, \;\; k > 0. \tag{54}$$

Given the condition expressed earlier, we conclude that at least one of the roots has a positive real part. This is due to the fact that $E_t < -\beta^2 T_0/\rho c$ implies that $\rho c E_t + \beta^2 T_0 < 0$, which in return leads to $D(0) < 0$. Meanwhile, $\lim_{x\to\infty} D(x) > 0$, as the characteristic polynomial of Eq. (49) is monic. According to the intermediate value theorem (or more specifically Bolzano's theorem, cf. [55]), the two aforementioned conditions combining the fact that the polynomial with real coefficients is continuous imply that Eq. (49) has at least one root with positive real part. Thus, there are two possible sets of solutions of $D(\lambda)$: (i) one positive real root and a pair of complex conjugate roots and (ii) three real roots in which at least one is positive. As discussed in Zhang *et al*. [29], the first case enables waves to propagate by remaining the governing equations to be hyperbolic under strain softening condition. In the second case, however, the wave speed becomes imaginary, which leads the dynamic governing equations to be elliptic: the finite element analysis will show mesh dependency [29]. Therefore, we evaluate the cubic polynomial of Eq. (49) to have one real root and a pair of complex conjugate roots by considering that the discriminant (denoted as, $\triangle$) should be less than zero. According to Eqs. (49) to (53), the discriminant of cubic function can be expressed as

$$\triangle = -4{b^0}^3 y^3 + {a^0}^2 {b^0}^2 y^4 + 18 a^0 b^0 c^0 y^4 - 27{c^0}^2 y^4 - 4{a^0}^3 c^0 y^5. \tag{55}$$

This expression can be rewritten in terms of coefficients, w, r, and s, that is,

$$\triangle = -y^3(wy^2 + ry + s), \tag{56}$$

where

$$w = 4{a^0}^3 c^0, \tag{57}$$

$$r = 27{c^0}^2 - {a^0}^2 {b^0}^2 - 18 a^0 b^0 c^0, \tag{58}$$

$$s = 4{b^0}^3. \tag{59}$$

To keep the discriminant ($\triangle$) negative, we note that the quadratic polynomial of $wy^2 + ry + s$ in Eq. (56) should be always positive. Under the given condition in Eq. (54), we know that the coefficient w becomes negative because c^0 is negative and a^0 is positive. Besides, we can find out

DOI: 10.1002/nag

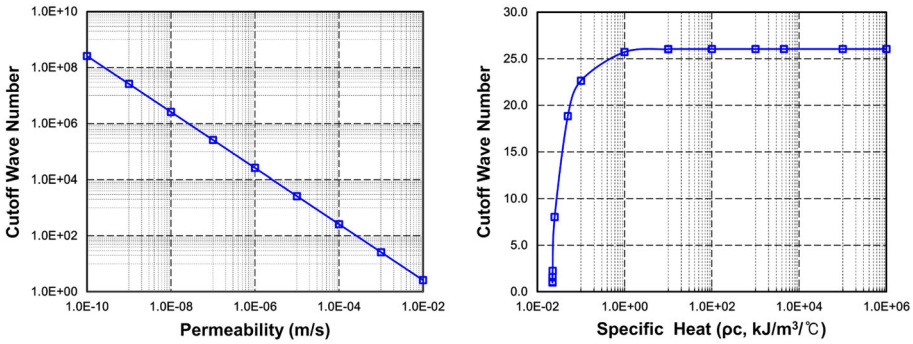

(a) Cutoff wavenumber vs. Permeability ($\rho c = 4.5kJ/m^3/^\circ C$) **(b)** Cutoff wavenumber vs. Specific Heat ($k_{perm} = 1.0 \times 10^{-3}$ m/s)

Figure 2. Relationship of the cutoff wavenumber with permeability and specific heat under adiabatic condition.

that s becomes positive because b^0 is come to be positive as proved in Appendix B. Therefore, we can derive the only positive root of $wy^2 + ry + s = 0$ in the form of $(-r - \sqrt{r^2 - 4ws})/2w$ based on the fact that $w < 0$ and $s > 0$. In other words, this makes Eq. (56) be always negative ($\triangle < 0$) when the square of the wavenumber y ($= k_w^2$) is within the range described as follows:

$$0 < y < \frac{-r - \sqrt{r^2 - 4ws}}{2w} \left(= k_{w,cut}^2\right). \tag{60}$$

The cutoff wavenumber ($k_{w,cut}$) as a function of the permeability or mobility (k), specific heat (ρc), tangential modulus (E_t), reference temperature (T_0), and other material properties of porous media has also been sought in this study. Because of the length of the derivation, the step-by-step derivation that leads to the expression of the cutoff wavenumber is provided in Appendix B. Meanwhile, the influences of the permeability and specific heat on the cutoff wavenumber are depicted in Figure 2. The reciprocal of permeability shows a linear relation to the cutoff wavenumber in log-log plane; however, the specific heat shows limited effect until it reaches to 1.0. In this regard, we can find out that the permeability is closely related to the cutoff wavenumber, while the specific heat has little influence on it.

Within the range of cutoff wavenumber, three roots (one real and two complex conjugate roots) of the third-order characteristic equation can be determined by Cardano's formula. By letting $\lambda = z - \frac{a}{3}$, the third-order polynomial Eq. (49) can be rewritten as

$$z^3 + pz + q = 0, \tag{61}$$

where

$$p = \frac{1}{3}(3b - a^2), \quad q = \frac{1}{27}(2a^3 - 9ab + 27c). \tag{62}$$

This equation has three roots that take the following forms,

$$z_1 = A + B, \quad z_{2,3} = -\frac{A + B}{2} \pm \frac{i\sqrt{3}}{2}(A - B), \tag{63}$$

where

$$A = \sqrt[3]{-\frac{q}{2} + \sqrt{\frac{q^2}{4} + \frac{p^3}{27}}}, \quad B = \sqrt[3]{-\frac{q}{2} - \sqrt{\frac{q^2}{4} + \frac{p^3}{27}}}. \tag{64}$$

Therefore, we can rewrite the solution λ as follows,

$$\lambda_1 = (A + B) - \frac{a}{3}, \quad \lambda_{2,3} = -\frac{A + B}{2} + \frac{i\sqrt{3}}{2}(A - B) - \frac{a}{3}, \tag{65}$$

DOI: 10.1002/nag

and distinguish the real part and imaginary part in the roots:

$$\lambda_r = -\frac{1}{2}(A+B) - \frac{a}{3},\ \lambda_i = \frac{\sqrt{3}}{2}(A-B). \tag{66}$$

By substituting the complex root into the damped harmonic equation like we did before in Eq. (43), we have (note that $\lambda_i = \omega$):

$$v(x,t) = Ae^{ik_w x}e^{\lambda_r t - i\omega t} = Ae^{ik_w x}e^{\lambda_r t - i\lambda_i t},\ \ v = [u, p, T]^T. \tag{67}$$

Recall the relation between the phase velocity v_p and the wavenumber k_w,

$$v_p = \frac{|\lambda_i|}{k_w}. \tag{68}$$

By means of $t = x/v_p$, the damping term $e^{(\lambda_r)t}$ changes into $e^{k_w((\lambda_r)/|\lambda_i|)x} = e^{-\alpha x}$, where α is the damping coefficient [29]. Notice that the THM coupling introduces rate dependence to the mechanical response, even if the solid phase continuum does not exhibit any viscous behavior. As a result of this rate dependence, the internal length scale l is introduced, that is,

$$l = \alpha^{-1},\quad \alpha = -\frac{\lambda_r}{|\lambda_i|}k_w, \tag{69}$$

in which λ_r and λ_i are obtained from Eq. (66). It is obvious that the definition of internal length scale holds only for dynamic analysis. The damping coefficient α and the internal length scale l can be expressed as shown in the succeeding equation:

$$\alpha = \frac{\left|A+B+\frac{2}{3}a\right|k_w}{\sqrt{3}(A-B)},\ \ l = \frac{\sqrt{3}(A-B)}{\left|A+B+\frac{2}{3}a\right|k_w}. \tag{70}$$

Therefore, we can identify the internal length scale as a function of the mobility (k), specific heat (ρc), wavenumber (k_w), reference temperature (T_0), tangential modulus under strain softening (E_t), and other material properties as follows:

$$l = f\left(k, \rho c, k_w, E_t, M, \beta, \alpha_m, T_0\right). \tag{71}$$

For brevity, the expression of the internal length scale is described in details in the Appendix C.

Remark 2
In the adiabatic condition, we derived the cutoff wavenumber, which guarantees the wave propagation is possible. Within this range, we can analyze how the damping coefficient changes along the wavenumber by normalizing it with the cutoff wavenumber in Figure 3.

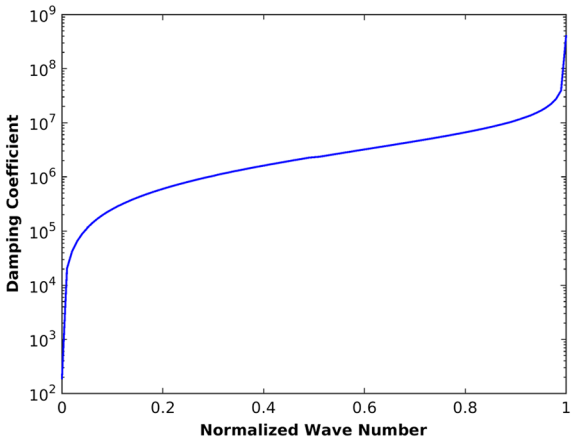

Figure 3. Damping coefficient (α) versus normalized wavenumber.

DOI: 10.1002/nag

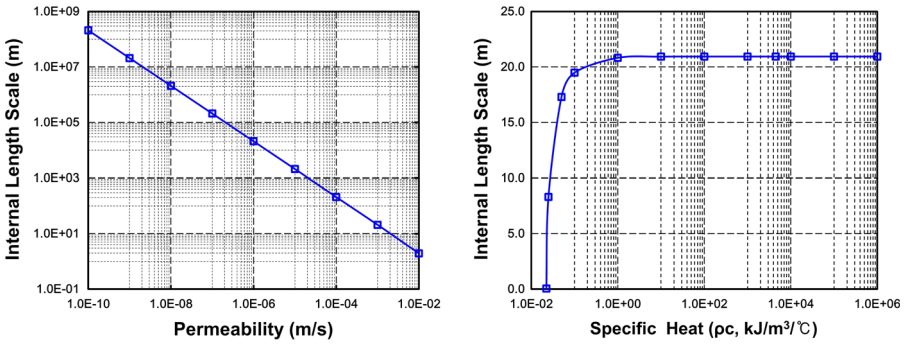

(a) Internal length scale vs. Permeability ($\rho c = 4.5kJ/m^3/°C$) **(b)** Internal length scale vs. Specific Heat ($k_{perm} = 1.0 \times 10^{-3}$ m/s)

Figure 4. Relationship of the internal length scale with the permeability and specific heat under the adiabatic condition.

In this figure, we can see that the damping coefficient (α) approaches zero when the wavenumber decreases, which is natural phenomenon considering the definition of α. On the other hand, the damping coefficient approaches to infinity when the wavenumber converges to the cutoff value, which states that the internal length scale, a reciprocal of α, vanishes. This fact is also analogous to the case of long wavelength limit under the non-isothermal condition, Eq. (48). The effect of permeability (or mobility, k) and specific heat (ρc) of porous media on the internal length scale is compared in Figure 4. We can see that the permeability has proportional relation to the internal length scale while the specific heat has limited effect.

3. NUMERICAL EXPERIMENTS

To illustrate the influences of THM coupling on the width of localization zone, we use an implicit dynamic finite element code to simulate one-dimensional wave propagation in a thermo-sensitive fully saturated porous bar with different set of material parameters. Our objective here is to use the numerical experiments to (i) verify the theoretical analysis on the phase velocity and internal length scales in Section 2.2 and (ii) confirm whether mesh dependency occurs when the physical internal length scale is predicted to be vanished according to Eqs. (48) and (71).

As mentioned previously in Section 2.3.1, we did not obtain the expression of internal length scale for the non-isothermal condition, as the general algebraic expression of the internal length scale does not exist according to the Abel–Ruffini theorem [54]. As a result, we first limit our focus on the adiabatic condition and performed numerical experiments to validate the analytical expression of the internal length scale. We then analyze the simulated wave propagation behavior of the non-isothermal condition with a series of numerical simulations under the different thermal conductivities. The changes of wave propagation behaviors observed in the numerical simulations due to changes of the thermal conductivity are also compared. We found that the observed behavior is consistent with the phase velocity expressed in Eq. (47).

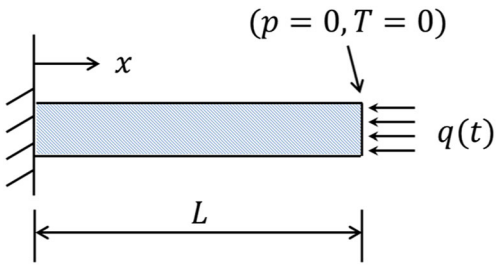

Figure 5. One dimensional soil bar in axial compression

DOI: 10.1002/nag

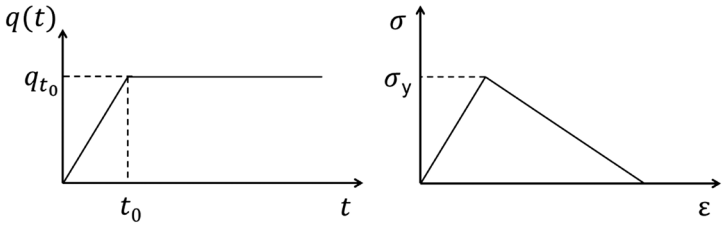

Figure 6. Applied stress and local stress-strain diagram

The numerical model consists of a softening bar constrained to move in only one direction. In addition, heat transfer and pore-fluid diffusion are also confined to be one-dimensional. The length of the bar is 10 m. At $x = 0$ m, the bar is fixed and has zero displacement, while a perturbation of force is applied at $x = 10$ m. Both pore pressure and temperature are prescribed as zero at $x = 10$ m. A constant time step $\triangle t = 1.0 \times 10^{-2}$ s is used to all the numerical simulations. The absolute mass densities of soil and fluid are selected as $\rho_s = 2,700$ kg/m^3 and $\rho_f = 1,000$ kg/m^3. The elastic and tangential moduli under strain softening are assumed to be 30 and -20 MPa, respectively, and the Biot's modulus (M) is considered to be 200 MPa. The reference temperature T_0 is set to be 20 $^\circ C$, and the numerical condition of applied stress and local stress-strain diagram are depicted with boundary conditions in Figures 5 and 6. Here, t_0 is set to be 0.1 s, q_{t_0} is applied as 500 kPa, and σ_y values are indicated in the figures for each simulation.

3.1. Adiabatic case

The reference case of internal length scale under the adiabatic condition is calculated with the permeability (k_{perm}) of 5.0×10^{-3} m/s and the specific heat (ρc) of 4.5 kJ/m^3/°C. The internal length of each case is described in the following Table II when the wavenumber is assumed to be unity. The numerical simulations are investigated with the element size of 0.4 m.

The reference case gives the internal length scale of 4.10 m, and the plastic wave is able to propagate. We can verify this from the numerical simulation results depicted in Figure 7. Nevertheless, in another two numerical experiments, one with increased permeability and the other

Table II. The internal length scale under the different conditions (Adiabatic case).

k_{perm}(m/s)	ρc(kJ/m^3/°C)	l(m)($k_w = 1.0$)	Comparison
5.0×10^{-3}	4.5	4.10	the reference
2.5×10^{-2}	4.5	0.19	permeability change
5.0×10^{-3}	2.4×10^{-2}	0.94	specific heat change

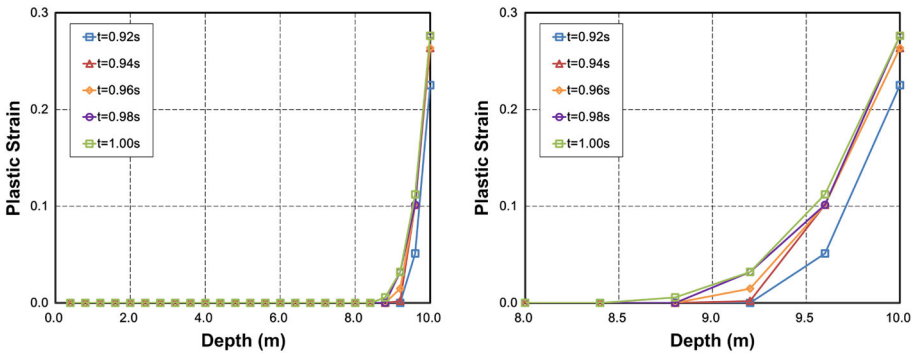

Figure 7. Developement of the localization zone under possible wave propagation – the plastic strain moves towards the depth along the time (the reference condition, permeability $= 5.0 \times 10^{-3}$ m/s, $\rho c = 4.5$ kJ/m^3/°C, σ_y =30 MPa)

DOI: 10.1002/nag

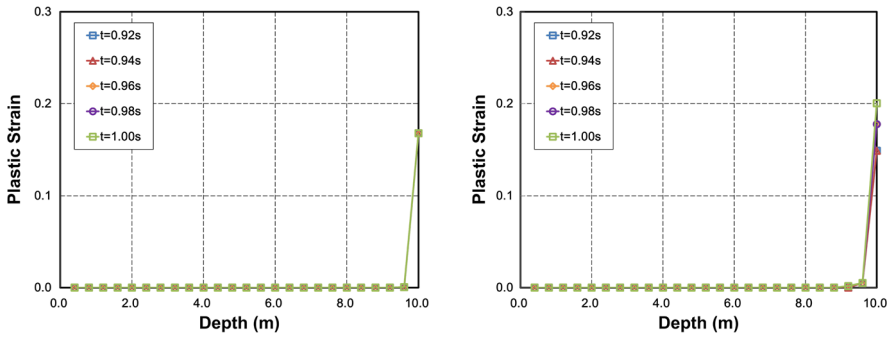

(a) Permeability change ($k_{perm} = 2.5\times10^{-2}$m/s, $\sigma_y = 34$ MPa) **(b)** Specific heat change ($\rho c = 2.2\times10^{-2} kJ/m^3/°C$, $\sigma_y = 30$ MPa)

Figure 8. Development of the localization zone under no wave propagation – the plastic strain stays at the same depth along the time

with lowered specific heat, the harmonic wave ceases to propagate and the plastic zone seizes at a certain depth as shown in Figure 8. This fixed plastic zone with time indicates that the wave is unable to propagate. This observation is consistent with Eq. (70), and the relationship among the internal length scale, permeability, and specific heat showcased in Figure 4. Similar plastic strain patterns were noticed by Zhang *et al*. [29] in dynamic wave propagation simulations under the isothermal condition.

3.2. Non-isothermal case

With the results shown in Figure 7 as the reference, we vary the thermal conductivity and determine how the thermal conductivity affects wave propagation. We assumed that the thermal conductivities of fluid and solid are the same and selected the value from the previous study by Sun [22], $\kappa = 2.5\times 10^{-3}$ kW/m/°C. According to our previous analysis, both thermal conductivity and permeability can influence on the behavior of the THM system (Figure 1). In order to analyze this effect, we conducted parametric study of thermal conductivity under two permeability conditions: (i) 5.0×10^{-3} m/s from the reference case in Section 3.1 and (ii) 1.0×10^{-10} m/s as low permeability case. A series of numerical simulations are performed by varying the thermal conductivities provided that the specific heat (ρc) is assumed to be 4.5 kW/m/°C.

Firstly, we introduced the thermal conductivity into the reference case and conducted the numerical simulation. When $\kappa = 2.5 \times 10^{-3}$ kW/m/°C was adopted, the numerical simulation showed little change in the plastic strain compared with the adiabatic condition in Figure 7. However, when the thermal conductivity is increased to 1.0 kW/m/°C, we found the wave propagation behavior started to change. These results are depicted in Figure 9. The plastic strain is increased compared with the adiabatic case, and the plastic wave is still able to propagate along time. Considering the

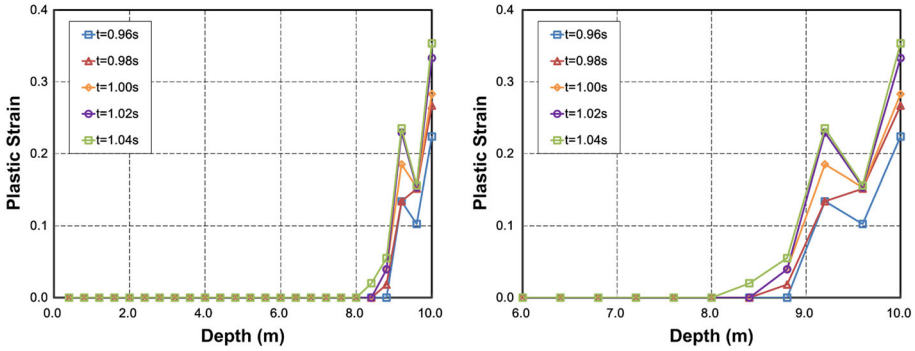

Figure 9. Developement of the localization zone (non-isothermal condition with $\kappa = 1.0$ kW/m/°C, $\sigma_y = 30$ MPa).

DOI: 10.1002/nag

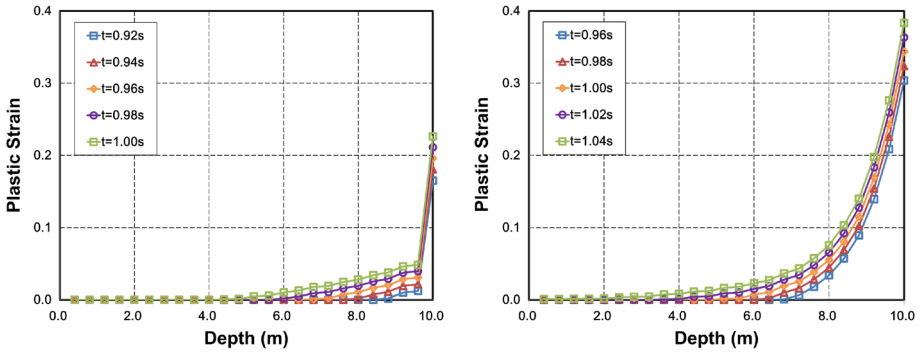

(a) $\kappa = 2.5 \times 10^{-3}$ kW/m/°C **(b)** $\kappa = 1.0$ kW/m/°C

Figure 10. Developement of the localization zone of non-isothermal condition with different thermal conductivities – plastic zone moves toward the depth along the time ($k_{perm} = 1.0 \times 10^{-10}$ m/s, $\rho c = 3.5$ kW/m/°C, $\sigma_y = 3.8$ MPa).

initial and boundary conditions of temperature field, we expect that the prescribed zero temperature at the surface (10 m) contributes additional compression to the one-dimensional bar.

Next, we started from the numerical set up of adiabatic limit with the permeability equal to 1.0×10^{-10} m/s. When the thermal conductivity of 2.5×10^{-3} kW/m/°C was applied, the response of plastic strain gave little effects compared with the adiabatic condition. When κ became larger than 1.0×10^{-1} kW/m/°C, however, we found the changes of plastic localization zone. Figure 10 depicts the changes of wave propagation with different thermal conductivities under the low permeability condition. We can identify that both permeability and thermal conductivity influence on the behavior of wave propagation under strain softening from Figures 9 and 10.

Furthermore, we took two cases in Section 3.1, in which the wave was not able to propagate, and re-analyzed the simulations by introducing the thermal conductivity. Again, the thermal conductivity of 2.5×10^{-3} kW/m/°C showed little effect on both cases. Figure 11 shows when $\kappa = 1.0$ kW/m/°C was applied. We can see the width of localization zones, and the plastic strains are increased compared with adiabatic case in Figure 8. However, the plastic wave does not propagate along time. This indicates that the thermal conductivity appears limited effect on regularization.

Remark 3

We conducted additional numerical simulations for the non-isothermal case to analyze the influence of mesh size on shear band width. The permeability of 1.0×10^{-10} m/s was selected to have enough internal length scale for stability. The thermal conductivity ($\kappa = 2.5 \times 10^{-3}$ kW/m/°C) and the specific heat ($\rho c = 4.5$ kJ/m^3/°C) were adopted from the previous study by Sun [22]. The one-dimensional domain was discretized by 10, 20, 25, 30 linear finite element of equal sizes to

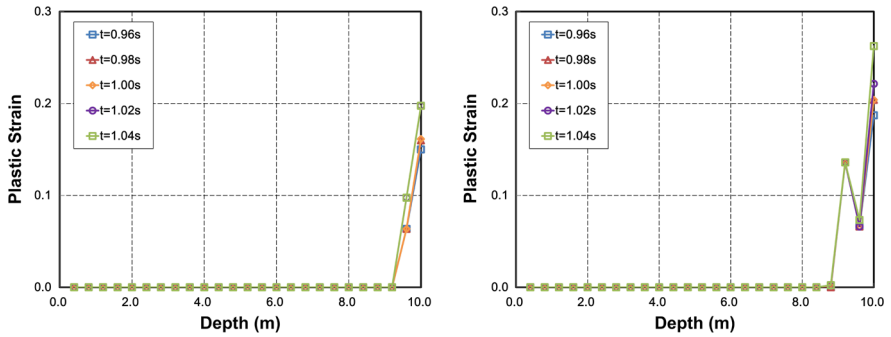

(a) Permeability change ($k_{perm} = 1.0 \times 10^{-2}$m/s, $\sigma_y = 34$ MPa) **(b)** Specific heat change ($\rho c = 2.2 \times 10^{-2}$ kJ/m^3/°C, $\sigma_y = 30$ MPa)

Figure 11. Development of the localization zone under no wave propagation – the plastic strain stays the same depth along the time (non-isothermal condition, $\kappa = 1.0$ kW/m/°C)

DOI: 10.1002/nag

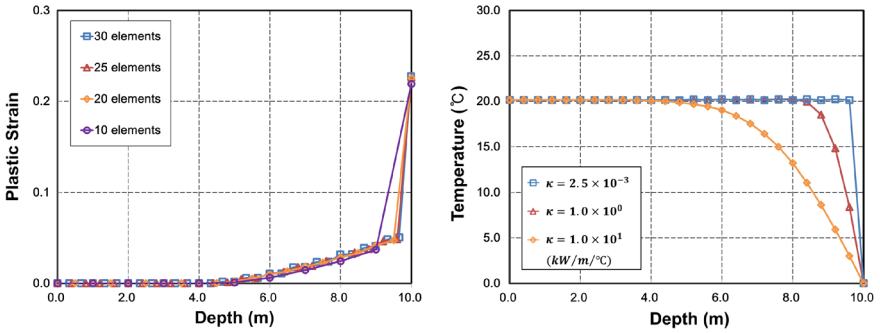

(a) Plastic strain along the bar under different mesh conditions ($\kappa = 2.5 \times 10^{-3}$kW/m/°C)

(b) Temperature field results under different thermal conductivities (with 25 elements)

Figure 12. Independence of the strain localization zone width under different mesh sizes and limited changes of temperature field along the bar under various thermal conductivities (at $t = 1.0$ s with $k_{perm} = 1.0 \times 10^{-10}$ m/s, $\rho c = 4.5$ kJ/m^3/°C).

study mesh dependency. As shown in Figure 12(a), the plastic strain distribution from the numerical simulations suggests mesh independence. In addition, Figure 12(b) describes temperature field distribution of the numerical simulations for the non-isothermal condition. With the same material properties used in the mesh study, the domain with 25 elements is selected. We can see how the temperature changes with different thermal conductivities.

4. CONCLUSION

The one-dimensional wave propagation in a full saturated, thermo-sensitive porous medium has been analyzed. The stability analysis indicates that the governing equations of the thermo-hydro-mechanics system lead to a characteristic polynomial at least one order higher than the isothermal poromechanics counterpart. By applying the Routh–Hurwitz stability criterion to this higher-order characteristic polynomial, we determine that instability may occur if (i) strain softening occurs and/or (ii) specific heat per mass is less than a critical value proportional to Biot's modulus and the square of the thermal expansion coefficient, and (iii) when both permeability and thermal conductivity are 0. Dispersion analysis on the THM system reveals that a dispersive wave may propagate in a fully saturated, thermo-sensitive system under certain limited conditions. Nevertheless, the internal length scale introduced by the THM coupling vanishes at the short wavelength limit. For the adiabatic limit case, we derive an explicit expression of the internal length scale as a function of permeability, specific heat, wavenumber, and other material properties. The cutoff wavenumber is also identified. Our results indicate that there is a limited range of wavenumbers that allows dispersive waves to propagate at a finite speed.

APPENDIX A: RELATION BETWEEN PHASE VELOCITY AND WAVENUMBER

In the dispersion analysis of non-isothermal two-phase porous media, we may establish the relation between the phase velocity (v_p) and the wavenumber (k_w). Our starting point is Eq. $(45)_2$ from Section 2.3.1, which reads

$$\omega^2 = \frac{4a_4\lambda_r^3 + 3a_3\lambda_r^2 + 2a_2\lambda_r + a_1}{4a_4\lambda_r + a_3}, \tag{A.1}$$

where the coefficients are from Eqs. (17) to (20), that is,

$$a_4 = \rho(\rho c - 9\alpha_m^2 T_0 M), \tag{A.2}$$

$$a_3 = \rho(\kappa + \rho c k M)k_w^2, \tag{A.3}$$

DOI: 10.1002/nag

$$a_2 = (\rho c E_t + \rho c b^2 M + \rho \kappa k M k_w^2 + \beta^2 T_0 + 6\alpha_m \beta b T_0 M - 9 E_t \alpha_m^2 T_0 M) k_w^2, \tag{A.4}$$

$$a_1 = (E_t \kappa + b^2 \kappa M + \rho c E_t k M + \beta^2 k T_0 M) k_w^4. \tag{A.5}$$

By substituting Eqs. (A.2) to (A.5) in to Eq. (A.1), we may express ω in terms of wavenumber (k_w) as shown in the succeeding equation,

$$\omega^2 = \frac{a_{w4} + a_{w3} k_w^2 + a_{w2} k_w^4}{a_{w1} + a_{w0} k_w^2}, \tag{A.6}$$

where the coefficients in Eq. (A.6) are

$$a_{w4} = 4\rho \left(\rho c - 9\alpha_m^2 T_0 M\right) \lambda_r^3, \tag{A.7}$$

$$a_{w3} = 3\rho(\kappa + \rho c k M)\lambda_r^2 + 2\left(\rho c E_t + \rho c b^2 M + \beta^2 T_0 + 6\alpha_m \beta b T_0 M - 9 E_t \alpha_m^2 T_0 M\right) \lambda_r \tag{A.8}$$

$$a_{w2} = 2(\rho \kappa k M)\lambda_r + E_t \kappa + b^2 \kappa M + \rho c E_t k M + \beta^2 k T_0 M, \tag{A.9}$$

$$a_{w1} = 4\rho \left(\rho c - 9\alpha_m^2 T_0 M\right) \lambda_r, \tag{A.10}$$

$$a_{w0} = \rho(\kappa + \rho c k M). \tag{A.11}$$

Therefore, the phase velocity ($v_p = \omega / k_w$) can be expressed as a function of the wavenumber (k_w) and material parameters as shown in the succeeding equation,

$$v_p = \frac{\omega}{k_w} = \sqrt{\frac{a_{w4}/k_w^2 + a_{w3} + a_{w2} k_w^2}{a_{w1}/k_w^2 + a_{w0}}}. \tag{A.12}$$

This relation proves that the wave propagating in the porous media that has already lost stability is dispersive.

APPENDIX B: CUTOFF WAVENUMBER FOR THE ADIABATIC CASE

The objective of this section is to determine the cutoff wavenumber of the adiabatic THM system. At the adiabatic limit, the characteristic polynomial of the THM system takes the following form (the same with Eq. (49) to Eq. (53)),

$$\lambda^3 + a\lambda^2 + b\lambda + c = 0, \tag{B.1}$$

where the coefficients of the characteristic Eq. (B.1) reads

$$a = a^0 y, \;\; a^0 = \frac{\rho c k M}{\rho c - 9\alpha_m^2 T_0 M}, \tag{B.2}$$

$$b = b^0 y, \;\; b^0 = \frac{\rho c E_t + \rho c b^2 M + \beta^2 T_0 + 6\alpha_m \beta b T_0 M - 9\alpha_m^2 E_t T_0 M}{\rho(\rho c - 9\alpha_m^2 T_0 M)}, \tag{B.3}$$

$$c = c^0 y^2, \;\; c^0 = \frac{\left(\rho c E_t + \beta^2 T_0\right) k M}{\rho\left(\rho c - 9\alpha_m^2 T_0 M\right)}, \tag{B.4}$$

$$y = k_w^2. \tag{B.5}$$

The discriminant of the previous equations is denoted as

$$\triangle = -4{b^0}^3 y^3 + {a^0}^2 {b^0}^2 y^4 + 18 a^0 b^0 c^0 y^4 - 27 {c^0}^2 y^4 - 4{a^0}^3 c^0 y^5, \tag{B.6}$$

DOI: 10.1002/nag

which can be rewritten in terms of the coefficients, w, r, and s, that is,

$$\triangle = -y^3(wy^2 + ry + s), \tag{B.7}$$

where

$$w = 4a^{0\,3}c^0, \tag{B.8}$$

$$r = 27c^{0\,2} - a^{0\,2}b^{0\,2} - 18a^0b^0c^0, \tag{B.9}$$

$$s = 4b^{0\,3}. \tag{B.10}$$

Following the approach used in Section 2.3.2, we assume that stability of the adiabatic system has already lost and determine the cutoff wavenumber beyond which the dispersive wave fails to propagate at a finite speed. Assuming that the porous medium remains permeable, the condition that causes the adiabatic THM system losing stability reads

$$-b^2M < E_t < -\beta^2T_0/\rho c, \;\; c > 9\alpha_m^2T_0M/\rho, \;\; k > 0. \tag{B.11}$$

Assuming that Condition (B.11) holds, we may conclude that Eq. (B.1) has one real root and two complex conjugate roots if we can prove that the discriminant in Eq. (B.6) is negative. Note that the quadratic polynomial of $wy^2 + ry + s$ in Eq. (B.7) is positive when the wave can propagate, because y^3, a function of wavenumber (k_w), is always positive in that case. Furthermore, by applying Condition (B.11) into Eq. (B.4) and Eq. (B.5), one may deduce that c^0 is strictly negative and a^0 is strictly positive. Therefore, we conclude that the coefficient w is negative when Condition (B.11) holds. Next, we consider the term b^0. Assume that

$$b^0 = \frac{\rho cE_t + \rho cb^2M + \beta^2T_0 + 6\alpha_m\beta bT_0M - 9\alpha_m^2E_tT_0M}{\rho\left(\rho c - 9\alpha_m^2T_0M\right)} > 0. \tag{B.12}$$

This assumption implies that

$$\rho cE_t + \rho cb^2M + \beta^2T_0 + 6\alpha_m\beta bT_0M - 9\alpha_m^2E_tT_0M > 0, \quad \left(\because \rho c - 9\alpha_m^2T_0M > 0\right) \tag{B.13}$$

$$\Rightarrow \quad E_t > \frac{-\rho cb^2M - \beta^2T_0 - 6\alpha_m^2\beta bT_0M}{\rho c - 9\alpha_m^2T_0M} \geq \frac{-\rho cb^2M - \beta^2T_0 - 6\alpha_m^2\beta bT_0M}{\rho c}, \tag{B.14}$$

$$\Rightarrow \quad E_t > -b^2M - \left(\frac{\beta^2T_0 + 6\alpha_m^2\beta bT_0M}{\rho c}\right). \tag{B.15}$$

Given that $(\beta^2T_0 + 6\alpha_m^2\beta bT_0M)/\rho c \geq 0$, the assumption (B.12) is valid under Condition (B.11). Therefore, b^0 is positive, which in return implies that s is also positive (according to Eq. (B.10)). Because w and s are of opposite signs, the two distinct roots of the quadratic function of $wy^2 + ry + s = 0$ always have the real parts that are of opposite signs unless the discriminant of the quadratic equation equals to 0. Furthermore, the root with a real positive part reads $(-r - \sqrt{r^2 - 4ws})/2w$. Recall that our focus is on the case where the discriminant is negative. This situation is particularly interesting, because it leads to two distinct non-real complex roots whose real parts are of opposite signs. Therefore, we can derive the range of y in which the discriminant expressed in Eq. (B.6) is negative ($\triangle < 0$), that is,

$$0 < y\left(= k_w^2\right) < \frac{-r - \sqrt{r^2 - 4ws}}{2w}, \tag{B.16}$$

DOI: 10.1002/nag

where

$$w = 4a^{0\,3}c^{0}, \tag{B.17}$$

$$r = 27c^{0\,2} - a^{0\,2}b^{0\,2} - 18a^{0}b^{0}c^{0}, \tag{B.18}$$

$$s = 4b^{0\,3}. \tag{B.19}$$

As a result, the cutoff wavenumber can be written as

$$k_{w,cut} = \sqrt{\frac{-r - \sqrt{r^2 - 4ws}}{2w}}, \tag{B.20}$$

in which each coefficient $(w,\ r,\ s)$ reads

$$w = \frac{4k^4M^4\rho^2c^3\left(\rho cE_t + \beta^2T_0\right)}{\left(\rho c - 9\alpha_m^2MT_0\right)^4}, \tag{B.21}$$

$$\begin{aligned} r =& \frac{27k^2M^2\left(\rho cE_t + \beta^2T_0\right)^2}{\rho^2\left(\rho c - 9\alpha_m^2MT_0\right)^2} \\ &- \frac{18ck^2M^2\left(\rho cE_t + \beta^2T_0\right)\left(\rho cE_t + \rho cb^2M + \beta^2T_0 + 6\alpha_m b\beta MT_0 - 9\alpha_m^2E_tMT_0\right)}{\rho\left(\rho c - 9\alpha_m^2MT_0\right)^3} \\ &- \frac{c^2k^2M^2\left(\rho cE_t + \rho cb^2M + \beta^2T_0 + 6\alpha_m b\beta MT_0 - 9\alpha_m^2E_tMT_0\right)^2}{(\rho c - 9\alpha_m^2MT_0)^4}, \end{aligned} \tag{B.22}$$

$$s = \frac{4\left(\rho cE_t + \rho cb^2M + \beta^2T_0 + 6\alpha_m b\beta MT_0 - 9\alpha_m^2E_tMT_0\right)^3}{\rho^3\left(\rho c - 9\alpha_m^2MT_0\right)^3}. \tag{B.23}$$

As a result, the cutoff wavenumber can be expressed as a function of mobility (k), specific heat (ρc), tangential modulus under strain softening (E_t), reference temperature (T_0), and other material parameters:

$$k_{w,cut} = f\left(k, \rho c, E_t, T_0, b, M, \beta, \alpha_m\right). \tag{B.24}$$

APPENDIX C: INTERNAL LENGTH SCALE FOR THE ADIABATIC CASE

The objective of this section is to determine the internal length scale of the adiabatic THM system. Considering the damping coefficient in Eq. (70), the coefficients in Eqs. (61) and (64) are written as follows:

$$\alpha = \frac{\left|A + B + \frac{2}{3}a\right|k_w}{\sqrt{3}(A - B)}, \tag{C.1}$$

where

$$A = \sqrt[3]{-\frac{q}{2} + \sqrt{\frac{q^2}{4} + \frac{p^3}{27}}}, \quad B = \sqrt[3]{-\frac{q}{2} - \sqrt{\frac{q^2}{4} + \frac{p^3}{27}}}, \tag{C.2}$$

DOI: 10.1002/nag

with

$$p = \frac{1}{3}(3b - a^2), \quad q = \frac{1}{27}(2a^3 - 9ab + 27c). \tag{C.3}$$

Here, we can express p, q in terms of material parameters:

$$p = \left[-\frac{k^2 M^2 \rho^2 c^2 k_w^4}{3(\rho c - 9\alpha_m^2 M T_0)^2} + \frac{\left(\rho c E_t + \rho c b^2 M + \beta^2 T_0 + 6\alpha_m \beta b M T_0 - 9\alpha_m^2 E_t M T_0\right) k_w^2}{\rho\left(\rho c - 9\alpha_m^2 M T_0\right)} \right], \tag{C.4}$$

$$\begin{aligned} q = \Bigg[& \frac{2\rho^3 c^3 k^3 M^3 k_w^6}{27\left(\rho c - 9\alpha_m^2 M T_0\right)^3} + \frac{kM\left(\rho c E_t + \beta^2 T_0\right) k_w^4}{\rho\left(\rho c - 9\alpha_m^2 M T_0\right)} \\ & - \frac{ckM\left(\rho c E_t + \rho c b^2 M + \beta^2 T_0 + 6\alpha_m \beta b M T_0 - 9\alpha_m^2 E_t M T_0\right) k_w^4}{3\left(\rho c - 9\alpha_m^2 M T_0\right)^2} \Bigg]. \end{aligned} \tag{C.5}$$

By rearranging the expression with respect to the permeability k, we can express the values of $-q/2$ and $q^2/4 + p^3/25$ in Eq. (C.2) as follows:

$$-\frac{q}{2} = a_{11} k + a_{12} k^3, \tag{C.6}$$

$$\frac{q^2}{4} + \frac{p^3}{27} = a_{21} + a_{22} k^2 + a_{23} k^4, \tag{C.7}$$

where

$$a_{11} = \left[-\frac{\rho c E_t + \beta^2 T_0}{2\rho\left(\rho c - 9\alpha_m^2 M T_0\right)} + \frac{c\left(\rho c E_t + \rho c b^2 M + \beta^2 T_0 + 6\alpha_m \beta b M T_0 - 9\alpha_m^2 E_t M T_0\right)}{6(\rho c - 9\alpha_m^2 M T_0)^2} \right] M k_w^4, \tag{C.8}$$

$$a_{12} = \left[-\frac{\rho^3 c^3}{27\left(\rho c - 9\alpha_m^2 M T_0\right)^3} \right] M^3 k_w^6, \tag{C.9}$$

$$a_{21} = \left[\frac{\left(\rho c E_t + \rho c b^2 M + \beta^2 T_0 + 6\alpha_m \beta b M T_0 - 9\alpha_m^2 E_t M T_0\right)^3}{27\rho^3\left(\rho c - 9\alpha_m^2 M T_0\right)^3} \right] k_w^6, \tag{C.10}$$

$$\begin{aligned} a_{22} = \Bigg[& \frac{\left(\rho c E_t + \beta^2 T_0\right)^2}{4\rho^2(\rho c - 9\alpha_m^2 M T_0)^2} - \frac{c\left(\rho c E_t + \beta^2 T_0\right)\left(\rho c E_t + \rho c b^2 M + \beta^2 T_0 + 6\alpha_m \beta b M T_0 - 9\alpha_m^2 E_t M T_0\right)}{6\rho\left(\rho c - 9\alpha_m^2 M T_0\right)^3} \\ & - \frac{c^2\left(\rho c E_t + \rho c b^2 M + \beta^2 T_0 + 6\alpha_m \beta b M T_0 - 9\alpha_m^2 E_t M T_0\right)^2}{108\left(\rho c - 9\alpha_m^2 M T_0\right)^4} \Bigg] M^2 k_w^8, \end{aligned} \tag{C.11}$$

$$a_{23} = \left[\frac{\rho^2 c^3\left(\rho c E_t + \beta^2 T_0\right)}{27\left(\rho c - 9\alpha_m^2 M T_0\right)^4} \right] M^4 k_w^{10}. \tag{C.12}$$

The damping coefficient α in Eq. (70) can be expressed as

DOI: 10.1002/nag

$$\alpha = \frac{k_w \left| A + B + \frac{2}{3}a \right|}{\sqrt{3}(A - B)} \quad \text{with} \quad a = a_{01}k \quad \text{and} \quad a_{01} = \left[\frac{\rho c M}{\rho c - 9\alpha_m^2 T_0 M} \right] k_w^2, \tag{C.13}$$

or equivalently as

$$\alpha = \frac{k_w \left| \sqrt[3]{a_{11} + a_{12}k^3 + \sqrt{a_{21} + a_{22}k^2 + a_{23}k^4}} + \sqrt[3]{a_{11} + a_{12}k^3 - \sqrt{a_{21} + a_{22}k^2 + a_{23}k^4}} + \frac{2}{3}a_{01}kk_w^2 \right|}{\sqrt{3}\left(\sqrt[3]{a_{11} + a_{12}k^3 + \sqrt{a_{21} + a_{22}k^2 + a_{23}k^4}} - \sqrt[3]{a_{11} + a_{12}k^3 - \sqrt{a_{21} + a_{22}k^2 + a_{23}k^4}} \right)}. \tag{C.14}$$

By adopting the small permeability as in the previous study [29], the limit form of Eq. (C.14) with respect to a small value of k is

$$\alpha \cong \frac{k_w \left| \sqrt[3]{a_{11} + \sqrt{a_{21}}} + \sqrt[3]{a_{11} - \sqrt{a_{21}}} + \frac{2}{3}a_{01}kk_w^2 \right|}{\sqrt{3}\left(\sqrt[3]{a_{11} + \sqrt{a_{21}}} - \sqrt[3]{a_{11} - \sqrt{a_{21}}} \right)}. \tag{C.15}$$

Therefore, the internal length scale (l), which is a reciprocal of the damping coefficient, can be calculated as a function of the mobility (k), specific heat (ρc), wavenumber (k_w), tangential modulus under strain softening (E_t), reference temperature (T_0), and other material properties as follows:

$$l = f(k, \rho c, k_w, E_t, M, \beta, \alpha_m, T_0) = \alpha^{-1} \cong \frac{\sqrt{3}\left(\sqrt[3]{a_{11} + \sqrt{a_{21}}} - \sqrt[3]{a_{11} - \sqrt{a_{21}}} \right)}{k_w \left| \sqrt[3]{a_{11} + \sqrt{a_{21}}} + \sqrt[3]{a_{11} - \sqrt{a_{21}}} + \frac{2}{3}a_{01}kk_w^2 \right|}. \tag{C.16}$$

ACKNOWLEDGEMENTS

This research is supported by the Earth Materials and Processes program at the US Army Research Office under grant contracts W911NF-14-1-0658 and W911NF-15-1-0581, as well as the Mechanics of Material program at National Science Foundation under grant contract CMMI-1462760. These supports are gratefully acknowledged. We thank the reviewers for their constructive suggestion and feedback.

REFERENCES

1. de Borst R, Crisfield M, Remmers JC, Verhoosel CV. *Nonlinear Finite Element Analysis of Solids and Structures*. John Wiley & Sons: Chichester, 2012.
2. Nádai A, Wahl AM. *Plasticity*. McGraw-Hill Book Company, Inc.: New York, 1931.
3. Bažant ZP, Oh BH. Crack band theory for fracture of concrete. *Matériaux et Construction* 1983; **16**(3):155–177.
4. Desrues J, Chambon R. Shear band analysis for granular materials: the question of incremental non-linearity. *Ingenieur-Archiv* 1989; **59**(3):187–196.
5. Rudnicki JW, Rice JR. Conditions for the localization of deformation in pressure-sensitive dilatant materials. *Journal of the Mechanics and Physics of Solids* 1975; **23**(6):371–394.
6. Sun WC, Andrade JE, Rudnicki JW, Eichhubl P. Connecting microstructural attributes and permeability from 3D tomographic images of *in situ* shear-enhanced compaction bands using multiscale computations. *Geophysical Research Letters* 2011; **38**(10).
7. Sun WC, Andrade JE, Rudnicki JW. Multiscale method for characterization of porous microstructures and their impact on macroscopic effective permeability. *International Journal for Numerical Methods in Engineering* 2011; **88**(12):1260–1279.
8. Sun WC, Ostien JT, Salinger AG. A stabilized assumed deformation gradient finite element formulation for strongly coupled poromechanical simulations at finite strain. *International Journal for Numerical and Analytical Methods in Geomechanics* 2013; **37**(16):2755–2788.
9. Sun WC. A unified method to predict diffuse and localized instabilities in sands. *Geomechanics and Geoengineering* 2013; **8**(2):65–75.
10. Hadamard J. *Propagation des ondes*. Chelsea Publishing Company: New York, 1949.

DOI: 10.1002/nag

11. Hill R. Acceleration waves in solids. *Journal of the Mechanics and Physics of Solids* 1962; **10**(1):1–16.
12. Needleman A. Material rate dependence and mesh sensitivity in localization problems. *Computer Methods in Applied Mechanics and Engineering* 1988; **67**(1):69–85.
13. Rice JR. On the stability of dilatant hardening for saturated rock masses. *Journal of Geophysical Research* 1975; **80**(11):1531–1536.
14. Hill R. A general theory of uniqueness and stability in elastic-plastic solids. *Journal of the Mechanics and Physics of Solids* 1958; **6**(3):236–249.
15. Bažant ZP, Belytschko T. Wave propagation in a strain-softening bar: exact solution. *Journal of Engineering Mechanics* 1985; **111**(3):381–389.
16. Lasry D, Belytschko T. Localization limiters in transient problems. *International Journal of Solids and Structures* 1988; **24**(6):581–597.
17. Runesson K, Ottosen NS, Dunja P. Discontinuous bifurcations of elastic-plastic solutions at plane stress and plane strain. *International Journal of Plasticity* 1991; **7**(1):99–121.
18. Sluys LJ. Wave propagation, localisation and dispersion in softening solids. *Ph.D. Thesis*, Delft University of Technology, Netherlands, 1992.
19. Sluys LJ, De Borst R, Mühlhaus HB. Wave propagation, localization and dispersion in a gradient-dependent medium. *International Journal of Solids and Structures* 1993; **30**(9):1153–1171.
20. Borja RI. Bifurcation of elastoplastic solids to shear band mode at finite strain. *Computer Methods in Applied Mechanics and Engineering* 2002; **191**(46):5287–5314.
21. Sun WC, Mota A. A multiscale overlapped coupling formulation for large-deformation strain localization. *Computational Mechanics* 2014; **54**(3):803–820.
22. Sun WC. A stabilized finite element formulation for monolithic thermo-hydro-mechanical simulations at finite strain. *International Journal for Numerical Methods in Engineering* 2015; **103**(11):798–839. DOI: 10.1002/nme.4910.
23. Belytschko T, Liu WK, Moran B, Elkhodary K. *Nonlinear Finite Elements for Continua and Structures*. John Wiley & Sons: Chichester, 2013.
24. Eringen AC. On nonlocal plasticity. *International Journal of Engineering Science* 1981; **19**(12):1461–1474.
25. Fish J, Chen W, Nagai G. Non-local dispersive model for wave propagation in heterogeneous media: one-dimensional case. *International Journal for Numerical Methods in Engineering* 2002; **54**(3):331–346.
26. Fish J. *Practical Multiscaling*. John Wiley & Sons: Chichester, 2013.
27. Zhang HW, Schrefler BA. Gradient-dependent plasticity model and dynamic strain localisation analysis of saturated and partially saturated porous media: one dimensional model. *European Journal of Mechanics-A/Solids* 2000; **19**(3):503–524.
28. Loret B, Prèvost JH. Dynamic strain localization in fluid-saturated porous media. *Journal of Engineering Mechanics* 1991; **117**(4):907–922.
29. Zhang HW, Sanavia L, Schrefler BA. An interal length scale in dynamic strain localization of multiphase porous media. *Mechanics of Cohesive-frictional Materials* 1999; **4**(5):443–460.
30. Schrefler BA, Majorana CE, Sanavia L. Shear band localization in saturated porous media. *Archives of Mechanics* 1995; **47**(3):577–599.
31. Schrefler BA, Sanavia L, Majorana CE. A multiphase medium model for localisation and postlocalisation simulation in geomaterials. *Mechanics of Cohesive-frictional Materials* 1996; **1**(1):95–114.
32. Benallal A, Comi C. On numerical analyses in the presence of unstable saturated porous materials. *International Journal for Numerical Methods in Engineering* 2003; **56**(6):883–910.
33. Abellan MA, de Borst R. Wave propagation and localisation in a softening two-phase medium. *Computer Methods in Applied Mechanics and Engineering* 2006; **195**(37):5011–5019.
34. Adam D, Markiewicz R. Energy from earth-coupled structures, foundations, tunnels and sewers. *Géotechnique* 2009; **59**(3):229–236.
35. Tsang CF, Stephansson O, Hudson JA. A discussion of thermo–hydro–mechanical (thm) processes associated with nuclear waste repositories. *International Journal of Rock Mechanics and Mining Sciences* 2000; **37**(1):397–402.
36. Shoop SA, Bigl SR. Moisture migration during freeze and thaw of unsaturated soils: modeling and large scale experiments. *Cold Regions Science and Technology* 1997; **25**(1):33–45.
37. Veveakis E, Vardoulakis I, Di Toro G. Thermoporomechanics of creeping landslides: The 1963 Vaiont slide, Northern Italy. *Journal of Geophysical Research: Earth Surface (2003–2012)* 2007; **112**(F3).
38. Zhang HW, Schrefler BA. Particular aspects of internal length scales in strain localization analysis of multiphase porous materials. *Computer methods in applied mechanics and engineering* 2004; **193**(27):2867–2884.
39. Biot MA. Variational Lagrangian-thermodynamics of nonisothermal finite strain mechanics of porous solids and thermomolecular diffusion. *International Journal of Solids and Structures* 1977; **13**(6):579–597.
40. McTigue DF. Thermoelastic response of fluid-saturated porous rock. *Journal of Geophysical Research: Solid Earth (1978–2012)* 1986; **91**:9533–9542.
41. Coussy O. *Poromechanics*. John Wiley & Sons: Chichester, 2004.
42. Belotserkovets A, Prèvost JH. Thermoporoelastic response of a fluid-saturated porous sphere: An analytical solution. *International Journal of Engineering Science* 2011; **49**(12):1415–1423.
43. Selvadurai APS, Suvorov AP. Boundary heating of poro-elastic and poro-elasto-plastic spheres. *Proceedings of the Royal Society of London A: Mathematical, Physical and Engineering Sciences* 2012; **468**(2145):2779–2806.
44. Zienkiewicz OC, Chan AHC, Pastor M, Schrefler BA, Shiomi T. *Computational Geomechanics*. Wiley: Chichester, 1999.

DOI: 10.1002/nag

45. Liu R, Wheeler MF, Dawson CN, Dean R. Modeling of convection-dominated thermoporomechanics problems using incomplete interior penalty Galerkin method. *Computer Methods in Applied Mechanics and Engineering* 2009; **198**(9):912–919.
46. Routh EJ. *A Treatise on the Stability of a Given State of Motion: Particularly Steady Motion*. Macmillan and Company: London, 1877.
47. Hurwitz A. Ueber die bedingungen, unter welchen eine gleichung nur wurzeln mit negativen reellen theilen besitzt. *Mathematische Annalen* 1895; **46**(2):273–284.
48. Selvadurai APS, Suvorov AP. Thermo-poromechanics of a fluid-filled cavity in a fluid-saturated geomaterial. *Proceedings of the Royal Society of London A: Mathematical, Physical and Engineering Sciences* 2014; **470**(2163). http://rspa.royalsocietypublishing.org/content/470/2163/20130634.
49. Benallal A, Comi C. Material instabilities in inelastic saturated porous media under dynamic loadings. *International Journal of Solids and Structures* 2002; **39**(13):3693–3716.
50. Biot MA. Theory of propagation of elastic waves in a fluid-saturated porous solid. I. low-frequency range. *The Journal of the Acoustical Society of America* 1956; **28**(2):168–178.
51. Simoes FMF, Martins JAC, Loret B. Instabilities in elastic–plastic fluid-saturated porous media: harmonic wave versus acceleration wave analyses. *International Journal of Solids and Structures* 1999; **36**(9):1277–1295.
52. Rizzi E, Loret B. Strain localization in fluid-saturated anisotropic elastic–plastic porous media. *International Journal of Engineering Science* 1999; **37**(2):235–251.
53. Sluys LJ, de Borst R. Wave propagation and localization in a rate-dependent cracked medium – model formulation and one-dimensional examples. *International Journal of Solids and Structures* 1992; **29**(23):2945–2958.
54. Abel NH. Beweis der unmöglichkeit, algebraische gleichungen von höheren graden als dem vierten allgemein aufzulösen. *Journal FÜR Die Reine und Angewandte Mathematik* 1826; **1**:65–84.
55. Morales CH. A Bolzano's theorem in the new millennium. *Nonlinear Analysis: Theory, Methods & Applications* 2002; **51**(4):679–691.

DOI: 10.1002/nag